Supplement of Atmos. Chem. Phys., 19, 6579–6594, 2019
https://doi.org/10.5194/acp-19-6579-2019-supplement

Supplement of

Photooxidants from brown carbon and other chromophores in illuminated particle extracts

Richie Kaur et al.

Correspondence to: Cort Anastasio (canastasio@ucdavis.edu)

Table of Contents

1. Text Sections

2. Tables and Figures

Table S1. Sample collection details and light absorption of particle extracts

Sample ID	Collection Dates	Collection Times [d]	Average hourly $PM_{2.5}$ concentration [e] ($\mu g/m^3$-air)	α_{300} [f] (cm^{-1})	Average Mass of PM extracted [g]	R_{abs} (300-450nm) [h] (10^{-6} mol-photons L^{-1} s^{-1})	$f_{Rabs\ IN}$ [i]	MAC_{DOC} (300 nm) [j] (10^4 cm^2 g^{-1}-C)	AAE [k]	Light Screening Factor [l]
Particle Extracts										
PME1*[a]	01/06/16 - 01/08/16	17:30 - 07:30 (N)	5.8 (2.1)	0.077	105 (16)	1.7	0.00080	2.6	6.8	0.98
PME2*[a]	12/18/15 - 12/20/15	17:30 - 07:30 (N)	15 (10)	0.100	269 (30)	1.8	0.0059	2.0	7.2	0.97
PME3[b]	01/26/16 - 01/29/16	10:20 - 09:45 (C)	16 (11)	0.272	328 (19)	4.2	0.0076	1.3	7.9	0.93
PME4 [b]	12/16/15 - 12/18/15	17:30 - 07:30 (N)	20 (8)	0.567	350 (14)	12	0.0031	2.6	6.4	0.85
PME5 [b]	01/10/16 - 01/12/16	17:30 - 07:30 (N)	5.9 (3.4)	0.317	132 (11)	7.4	0.00080	2.6	6.2	0.91
PME6 [b]	01/23/16 - 01/26/16	17:30 - 07:30 (N)	6.8 (2.9)	0.584	174 (14)	13	0.00058	3.0	6.9	0.84
PME3D0.5 [c]				0.556	323 (21)	8.8			7.7	0.87
PME3D1.3 [c]				0.199	315 (23)	3.2	0.0071	1.3	7.6	0.95
PME3D2.5* [a]				0.103	331 (15)	1.7	0.0092	1.3	7.6	0.97
PME3D10 [c]				0.0263	347	0.42	0.0062	1.3	7.6	0.99
Averages (±σ)										
"Standard" (PME3-6)				0.44 (0.16)		9.1 (4.1)	0.0030 (0.0033)	2.4 (0.7)	6.8 (0.7)	
"Dilute" (PME1*-2*,3D2.5*)				0.093 (0.014)		1.7 (0.1)	0.0053 (0.0042)	2.0 (0.6)	7.2 (0.4)	
Davis Fog [m]				0.094 (0.047)		1.8 (0.9)	0.0082 (0.0031)	1.3 (0.1)	6.6 (0.5)	
Test statistic [n]				**0.021**		**0.035**	0.061	**0.013**	0.56	
Field Blanks										
FB1[a]	12/18/15	09:38 - 09:40		0.0025	17.8 (7.6)	0.024				
FB2 [b]	01/20/16	10:08 - 10:10		0.0037	24.9 (9.1)	0.022				

[a] Samples extracted in 2.5 mL/filter square and referred to as the "dilute" extracts in the main text.

[b] PME3-6 were extracted as 1 mL/filter square and are referred to as "standard" extracts in the main text.

[c] PME3D0.5, PME3D1.3 and PME3D10 are extracts of sample PME3 using varying extraction volumes per filter square, namely 0.5 , 1.3 and 10 mL, respectively.

[d] N = Night-time samples, collected from 17:30 on one day until 07:30 AM the next day; this was done for consecutive days on the same filter. C = Continuous collection for the indicated number of days.

[e] Average (± 1σ) hourly $PM_{2.5}$ concentration for each sampling period measured at the UC Davis sampling site by the California Air Resources Board as reported on the *i*ADAM online database (California Air Resources Board, 2018).

[f] Base-10 absorbance of the extract (in cm^{-1}) at 300 nm.

[g] Average (± 1σ) mass of PM extracted from each filter square for a given sample.

[h] Rate of sunlight absorption by each extract in the 300 – 450 nm wavelength range (Eq. (2), main text).

[i] Fraction of calculated sunlight absorption due to inorganic nitrogen (nitrite and nitrate) in each sample. Equations are in Kaur and Anastasio (2017).

[j] Mass absorption coefficient of dissolved organic species at 300 nm for each sample (Eq. (3), main text) in units of 10^4 cm^{-2} g^{-1}-C.[l]

[k] Absorption Angstrom Exponent (AAE), calculated as the negative of the slope of a linear regression of the extract absorbance data between 300 and 450 nm versus the log of the wavelength: $\log(\mathrm{Abs}_{\lambda}) = \log(\mathrm{Abs}_{300}) - \mathrm{AAE} \times \log(\lambda)$, where λ is the wavelength and Abs_{λ} and Abs_{300} are the absorbance values at λ and 300 nm, respectively.

[l] Light-absorption-weighted internal screening factor, calculated as $S_{\lambda} = \frac{\sum[(1-10^{-\alpha_{\lambda} l}) \times I'_{\lambda}]}{\sum[(2.303 \times \alpha_{\lambda} l) \times I'_{\lambda}]}$. In this equation, α_{λ} is the pathlength-normalized absorbance of the extract at each wavelength, summed for the wavelength range in which light absorption by the extracts was the highest (280-350 nm); l is the pathlength of the quartz tube used for illuminating the extracts (0.4 cm); I'_{λ} is the actinic flux (mol-photons $\mathrm{L}^{-1}\ \mathrm{s}^{-1}$) of the illumination system, calculated using the photon count of the illumination system measured using a TIDAS Photo Diode Array Spectrometer and the measured pseudo-first-order rate constant for loss of our chemical actinometer, 2-nitrobenzaldehyde . The numerator represents the actual rate of light absorption by all chromophores in the extract while the denominator is the estimated rate of light absorption in the extract assuming it is low light-absorbing. A value of 1.0 indicates no light screening (Smith et al., 2014; Rehorek and Seidel, 1989).

[m] Average values previously measured in Davis fog samples (n = 4) (Kaur and Anastasio, 2017).

[n] Test statistic for comparison of standard PME and Davis fog averages: *p*-value for a two-tailed *t*-test for samples of unequal variance. Values below 0.05 are in bold.

Table S2. Chemical characteristics of particle extracts

Sample ID	DOC µM-C	[NO$_2^-$] µM	[NO$_3^-$] µM	[SO$_4^{2-}$] µM	[Cl$^-$] µM	[HCOO$^-$] µM	[NH$_4^+$] µM	[Na$^+$] µM	[K$^+$] µM	[Ca^{2+}] µM	[Mg^{2+}] µM
Particle Extracts											
PME1*[a]	562	0.29	113	12.5	15.7	2.1	55.3	82.3	29.9	2.5	0.0
PME2*[a]	900	2.8	884	31.3	19.8	4.1	751	78.9	43.0	8.3	2.3
PME3[b]	3610	10.2	2520	302	66.3	13.0	2580	343	171	22.1	3.3
PME4 [b]	4090	8.3	3290	91.1	69.6	21.4	2010	317	197	44.1	11.3
PME5 [b]	2350	3.8	375	22.9	36.7	10.9	287	287	76.7	9.8	2.2
PME6 [b]	3720	5.4	432	65.6	77.7	4.9	276	362	97.2	13.0	7.4
PME3D0.5 [c]	7132	18	4820	533	127	27	5052	681	342	53	6.4
PME3D1.3	2760	6.4	1830	216	48.2	10.5	1600	233	105	20.0	1.6
PME3D2.5 [a]	1400	4.1	1250	195	27.3	5.1	816	118	42.6	4.7	1.3
PME3D10	356	1.2	183	28.1	6.9	1.0	177	24.3	11.9	0.0	0.0
Averages (±σ)											
"Standard" (PME3-6)	3440 (760)	6.9 (2.9)	1650 (1480)	120 (124)	62.6 (17.9)	12.5 (6.8)	1290 (1190)	327 (33)	136 (58)	22.2 (15.5)	6.1 (4.1)
"Dilute" (PME1*-2*,3D2.5*)	953 (419)	2.4 (1.9)	749 (580)	80 (101)	20.9 (5.9)	3.8 (1.5)	541 (420)	93.2 (21.9)	38.5 (7.4)	5.2 (2.9)	1.2 (1.1)
Davis Fog	1240 (560)	3.4 (6.1)	1080 (630)	120 (84)	22.9 (13.0)	5.1 (2.6)	1070 (550)	- [d]	3.5 (1.9)	4.2 (1.1)	1.4 (0.4)
Test statistic [e]	**0.0042**	0.35	0.51	0.98	**0.013**	0.11	0.75	-	**0.019**	0.10	0.11
Field Blanks											
FB1[a]	78.9	0	4.5	0.8	9.0	1.1	3.1	63.8	8.3	1.4	0.0
FB2[b]	244	0	1.1	0.4	6.1	9.0	12.3	143.5	10.9	3.4	0.0
MQ	< DL	< DL	< DL	< DL	< DL	< DL	< DL	1.8	< DL	< DL	< DL

[a] Samples extracted in 2.5 mL/filter square and referred to as the "dilute" extracts in the main text.

[b] Samples extracted in 1mL/filter square and are referred to as "standard" extracts in the main text.

[c] DOC and IC values for sample PME3D0.5 were not measured due to a shortage of sample; instead, they were estimated by extrapolating the linear trends between these values and concentration factors for the other PME3 samples, namely, PME3, PME3D1.3, PME3D2.5 and PME3D10.

[d] Sodium could not be measured in the 2011 Davis fog samples due to high background sodium content .

[e] Test statistic for comparison of standard PME and Davis fog averages: *p*-value for a two-tailed *t*-test for samples of unequal variance. Values below 0.05 are in bold.

Table S3. Hydroxyl radical measurements

Sample ID	P_{OH} [a] 10^{-10} M s^{-1}	P_{OH} [a] μM h^{-1}	k'_{OH} [b] 10^{6} s^{-1}	τ_{OH} [c] μs	$[^{\bullet}OH]$ [d] 10^{-16} M	$10^{4} \times \Phi_{OH}$ [f]	$k'_{OH,org}$ / [DOC] [g] 10^{8} L (mol-C)$^{-1}$s^{-1}
Particle Extracts							
PME1*	1.0 (0.1)	0.37 (0.04)	0.63 (0.01)	1.6 (0.1)	1.7 (0.2)	0.62 (0.06)	11.1 (0.2)
PME2*	2.0 (0.2)	0.71 (0.07)	0.44 (0.04)	2.3 (0.2)	4.5 (0.6)	1.1 (0.1)	4.6 (0.4)
PME3	14.7 (0.3)	5.3 (0.1)	1.9 (0.4)	0.54 (0.13)	7.9 (1.9) [e]	3.5 (0.1)	4.9 (1.2)
PME4	14 (2)	5.2 (0.6)	2.3 (0.2)	0.43 (0.03)	6.3 (0.6)	1.2 (0.1)	5.4 (0.4)
PME5	4.6 (0.5)	1.7 (0.2)	1.6 (0.1)	0.62 (0.03)	2.8 (0.3)	0.63 (0.07)	6.8 (0.4)
PME6	13 (3)	4.8 (1.0)	4.0 (0.8)	0.25 (0.05)	3.3 (0.3)	1.1 (0.2)	11 (2)
PME3D0.5					7.3 (1.8) [e]		
PME3D1.3					3.0 (0.8) [e]		
PME3D2.5*	3.1 (0.1)	1.1 (0.02)	0.94 (0.29)	1.1 (0.3)	3.3 (1.0) [e]	1.86 (0.03)	6.4 (2.0)
PME3D10	0.47 (0.04)	0.17 (0.01)	0.071(0.031)	14 (6)	6.6 (2.8) [e]	1.1 (0.1)	1.7 (0.7)
Averages (±σ)							
“Standard” (PME3-6)	12 (5)	4.2 (1.7)	2.5 (1.1)	0.46 (0.16)	5.1 (2.4)	1.6 (1.3)	6.9 (2.6)
“Dilute” (PME1*-2*,3D2.5*)	2.0 (1.0)	0.73 (0.37)	0.67 (0.63)	1.6 (0.6)	3.2 (1.4)	1.2 (0.6)	7.4 (3.4)
Davis Fog	3.5 (1.0)	1.3 (0.3)	0.87 (0.31)	1.2 (0.4)	4.2 (0.7)	2.4 (1.7)	7.5 (3.2)
Test statistic [h]	**0.039**	**0.039**	0.058	**0.019**	0.51	0.47	0.79
Field Blanks [i]							
FB1 (dilute)	≤ 0.012	≤ 0.045	0.34 (0.04)	3.0 (0.4)			
FB2 (standard)	≤ 0.012	≤ 0.042	0.27 (0.01)	3.8 (0.2)			

Listed uncertainties (in parentheses) are ± 1 standard error from the errors in inverse plot (1/R^{*}_{p} vs. 1/[Benzene]) parameters, except for the averages (± 1σ)

All equations used for these calculations are discussed in Kaur and Anastasio (2017) unless otherwise stated.

* Samples extracted in 2.5 mL/filter square and referred to as the “dilute” extracts in the main text.

[a] Davis winter solstice-normalized rate of $^{\bullet}$OH photoproduction.

[b] Apparent pseudo-first rate constant for destruction of $^{\bullet}$OH due to natural sinks .

[c] Lifetime of $^{\bullet}$OH, calculated as $1/k'_{OH}$.

[d] Winter solstice-normalized steady-state concentration of $^{\bullet}$OH.

[e] $^{\bullet}$OH concentrations in PME3 and PME3D extracts were measured using MBO as a probe, corrected for loss due to quenching by MBO (discussed in Sect. S1). k'_{OH} for these samples was calculated as P_{OH} / $[^{\bullet}OH]$.

[f] Apparent quantum yield of $^{\bullet}$OH during simulated sunlight illumination, calculated as $\Phi_{OH} = P_{OH} / R_{abs.}$

[g] Ratio of $k'_{OH,org}$ (rate constant for loss of $^{\bullet}$OH due to organics only; Table S6) to the DOC concentration.

[h] Test statistic for comparison of standard PME and Davis fog averages: *p*-value for a two-tailed *t*-test for samples of unequal variance. Values below 0.05 are in bold.

[i] Blanks were analyzed by adding 1.5 mM benzene to an aliquot of the blank. Very little phenol formation was observed after 200 minutes of illumination in both blanks, which was used to calculate the upper limit $P_{\mathrm{OH.}}$

Table S4. Contributions of nitrite, nitrate and other sources to $^{\bullet}$OH photoproduction

Sample ID	$f_{POH,NO2^-}$ [a]	$f_{POH,NO3^-}$ [b]	$f_{POH,Other}$ [c]
Particle Extracts			
PME1*	0.072 (0.010)	0.15 (0.02)	0.78 (0.02)
PME2*	0.36 (0.05)	0.63 (0.09)	0.011 (0.010)
PME3	0.18 (0.02)	0.24 (0.02)	0.58 (0.03)
PME4	0.15 (0.02)	0.32 (0.05)	0.53 (0.05)
PME5	0.21 (0.03)	0.11 (0.02)	0.67 (0.04)
PME6	0.11 (0.03)	0.046 (0.011)	0.85 (0.03)
PME3D0.5	-	-	-
PME3D1.3	-	-	-
PME3D2.5*	0.35 (0.04)	0.57 (0.06)	0.084 (0.068)
PME3D10	0.67 (0.08)	0.55 (0.07)	-0.22 (0.11) [d]
Averages (±σ)			
"Standard" (PME3-6)	0.16 (0.05)	0.18 (0.12)	0.66 (0.14)
"Dilute" (PME1*-2*,3D2.5*)	0.26 (0.16)	0.45 (0.26)	0.29 (0.42)
Davis Fog	0.24 (0.40)	0.46 (0.29)	0.41 (0.41)

Listed uncertainties (in parentheses) are ± 1 standard error calculated from propagating errors in individual terms, except for the averages (± 1σ).

* Samples extracted in 2.5 mL/filter square and referred to as the "dilute" extracts in the main text.

[a] Fraction of $^{\bullet}$OH photoproduction rate attributable to nitrite. Calculated as ($j_{NO2\rightarrow OH} \times [NO_2^-]$)/ P_{OH} where the numerator is the rate of $^{\bullet}$OH photoproduction due to nitrite ($P_{OH,NO2}$), and is the product of the aqueous photolysis rate constant under Davis winter-solstice sunlight, $j_{NO2^-\rightarrow OH} = 2.6 \times 10^{-5}$ s^{-1} (Anastasio and McGregor, 2001), and the molar concentration of NO_2^- in each sample.

[b] Fraction •OH photoproduction rate attributable to nitrate. Calculated using an equation analogous to $f_{POH,NO2-}$, using aqueous nitrate photolysis rate constant, $j_{NO3^-\rightarrow OH} = 1.4 \times 10^{-7}$ s^{-1} (Anastasio and McGregor, 2001) and molar concentration of NO_3^- in each sample.

[c] Fraction of $^{\bullet}$OH photoproduction due to non-nitrite and –nitrate sources; calculated as ($P_{OH} - P_{OH,NO2-} - P_{OH,NO3-}$) / P_{OH}.

[d] $f_{POH,other}$ is negative for PME3D10 indicating that the total rate of $^{\bullet}$OH photoproduction is over-predicted using the measured molar NO_2^- and NO_3^- concentrations.

Table S5. Determination of chloride as an $^{\bullet}$OH sink, following procedure of Anastasio and Newberg (2007)

Sample ID	Measured k'_{OH} [c] $\mathrm{s^{-1}}$	$[\mathrm{Cl^-}]$ [d] M	$[\mathrm{H^+}]$ [e] M	$f_{\mathrm{Cl^-}\text{re-formed}}$ [f]	$k'_{\mathrm{OH,Cl^-}}$ [g] $\mathrm{s^{-1}}$	$f_{k\mathrm{OH,Cl^-}}$ [h]
PME1*[a]	6.3E+05	1.6E-05	6.31E-05	0.9997828	1.5E+01	2.3E-05
PME2*[a]	4.4E+05	2.0E-05	6.31E-05	0.99978	1.8E+01	4.2E-05
PME3	1.9E+06	6.6E-05	6.31E-05	0.99978	6.2E+01	3.3E-05
PME4	2.3E+06	7.0E-05	6.31E-05	0.99978	6.5E+01	2.8E-05
PME5	1.6E+06	3.7E-05	6.31E-05	0.999783	3.4E+01	2.1E-05
PME6	4.0E+06	7.8E-05	6.31E-05	0.99978	7.3E+01	1.8E-05
PME3D2.5*[a]	9.4E+05	2.7E-05	6.31E-05	0.99978	2.5E+01	2.7E-05
PME3D10[b]	7.1E+04	6.9E-06	6.31E-05	0.999783	6.4E+00	9.0E-05

[a] Samples PME1*, PME2*, PME3D2.5 were extracted in 2.5 mL Milli-Q per filter square, and are referred to as “dilute extracts” in the main text.

[b] PME3D10 was extracted in 10 mL Milli-Q per filter square.

[c] Measured pseudo-first order rate constant for loss of $^{\bullet}$OH.

[d] Measured chloride concentrations in the extracts.

[e] Hydrogen ion concentration. Since the extracts were acidified to pH 4.2, this value is constant across all extracts.

[f] Fraction of $\mathrm{Cl^-}$ reacting with $^{\bullet}$OH that ends up back as $\mathrm{Cl^-}$ and $^{\bullet}$OH. Values are calculated based on the reactions 1-4 below and the equation $f_{\mathrm{Cl^-}\text{re-formed}} = k_4/\left((k_2 \times [\mathrm{Cl^-}]) + (k_3 \times [\mathrm{H^+}]) + k_4\right)$

[g] Rate constant for loss of $^{\bullet}$OH due to $\mathrm{Cl^-}$ based on the fraction of reformed $\mathrm{Cl^-}$, calculated as $k'_{\mathrm{OH,Cl^-}} = (1 - f_{\mathrm{Cl^-}\text{re-formed}}) \times k_1$

[h] Fraction of measured k'_{OH} due to chloride.

(1) $^{\bullet}\mathrm{OH} + \mathrm{Cl^-} \rightarrow \mathrm{HOCl^{\bullet -}}$ $k_1 = 4.3\mathrm{E}{+}09\ \mathrm{M^{-1}s^{-1}}$

(2) $\mathrm{HOCl^{\bullet -}} + \mathrm{Cl^-} \rightarrow {}^{\bullet}\mathrm{Cl_2^-} + \mathrm{OH^-}$, $k_2 = 1.0\mathrm{E}{+}04\ \mathrm{M^{-1}s^{-1}}$

(3) $\mathrm{HOCl^{\bullet -}} + \mathrm{H^+} \rightarrow \mathrm{Cl^{\bullet}} + \mathrm{H_2O}$, $k_3 = 2.1\mathrm{E}{+}10\ \mathrm{M^{-1}s^{-1}}$

(4) $\mathrm{HOCl^{\bullet -}} \rightarrow \mathrm{Cl^-} + {}^{\bullet}\mathrm{OH}$, $k_4 = 6.4\mathrm{E}{+}09\ \mathrm{M^{-1}s^{-1}}$

Table S6. Contributions of nitrite, chloride and organics to k'_{OH}

Sample ID	Measured k'_{OH} [c] s^{-1}	$k'_{OH,NO2^-}$ [d] s^{-1}	k'_{OH,Cl^-} [e] s^{-1}	$k'_{OH,org}$ [f] s^{-1}	$f_{kOH,NO2^-}$ [g]	$f_{kOH,org}$ [h,i]
PME1* [a]	6.3E+05	2.9E+03	1.5E+01	6.2E+05	0.0046	1.0
PME2* [a]	4.4E+05	2.7E+04	1.8E+01	4.1E+05	0.063	0.94
PME3	1.9E+06	1.0E+05	6.2E+01	1.8E+06	0.055	0.95
PME4	2.3E+06	8.3E+04	6.5E+01	2.2E+06	0.036	0.96
PME5	1.6E+06	3.8E+04	3.4E+01	1.6E+06	0.023	0.98
PME6	4.0E+06	5.4E+04	7.3E+01	4.0E+06	0.013	0.99
PME3D2.5* [a]	9.4E+05	4.1E+04	2.5E+01	9.0E+05	0.044	0.96
PME3D10 [b]	7.1E+04	1.2E+04	6.4E+00	5.9E+04	0.16	0.83

[a] Samples PME1*, PME2*, and PME3D2.5* were extracted in 2.5 mL Milli-Q per filter square, and are referred to as “dilute extracts” in the main text.

[b] PME3D10 was extracted in 10 mL Milli-Q per filter square. All other extracts were extracted in 1.0 mL Milli-Q per filter square (standard extracts).

[c] Measured pseudo-first order rate constant for loss of $^{\bullet}OH$ (Table S3).

[d] Pseudo-first order rate constant for loss of $^{\bullet}OH$ due to nitrite. Value is calculated as $k'_{OH,NO2^-} = (k_{OH+NO2^-} \times [NO_2^-])$ where $k_{OH+NO2^-} = 1.1 \times 10^{10}$ M^{-1} s^{-1} (Barker et al., 1970).

[e] Pseudo-first order rate constant for loss of $^{\bullet}OH$ due to chloride. Value is calculated using the reaction between $^{\bullet}OH$ and Cl^- corrected for the fraction of the initial product $HOCl^{\bullet -}$ that fragments to reform $^{\bullet}OH$ and Cl^-, as discussed in Table S5 and Anastasio and Newberg (2007).

[f] Calculated pseudo-first-order rate constant for loss of $^{\bullet}OH$ due to organics, determined by subtracting the contribution of nitrite from the measured k'_{OH}. Contributions to k'_{OH} from common inorganic ions, including sulfate, nitrate, chloride, bicarbonate/carbonate (see footnote *h* below), and ammonium are negligible.

[g] Fraction of measured k'_{OH} due to nitrite.

[h] Fraction of measured $^{\bullet}OH$ sink due to organic species, estimated by subtracting the contributions due to nitrite from the measured value of k'_{OH}.

[i] The upper bound of the fraction of the measured k'_{OH} due to bicarbonate (HCO_3^-) and carbonate (CO_3^{2-}) was calculated to be 1.1×10^{-6} based on using the sample pH of 4.2 and assuming equilibrium with 400 ppm of atmospheric CO_2. This fraction was calculated based on the CO_2 equilibria 1-3 below (Seinfeld and Pandis, 2012), $k_{OH+HCO3^-} = 1 \times 10^7$ $M^{-1}s^{-1}$, and $k_{OH+CO32^-} = 4 \times 10^8$ $M^{-1}s^{-1}$ (Buxton et al., 1988b).

(1) $CO_2 \leftrightarrow CO_2.H_2O$ (aq), $K_{H*} = 3.4E\text{-}02$ M atm^{-1} (Physical Henry’s law constant)

(2) $CO_2.H_2O$ (aq) $\leftrightarrow H^+ + HCO_3^-$, $K_{a1} = 4.3E\text{-}07$ M (p$Ka1$ = 6.3)

(3) $HCO_3^- \leftrightarrow H^+ + CO_3^{2-}$, $K_{a2} = 4.7E\text{-}11$ M (p$Ka2$ = 10.3)

Thus, the contributions of HCO_3^- and CO_3^{2-} to measured k'_{OH} in all PME samples should be negligible.

Table S7. Singlet oxygen measurements

Sample ID	P_{1O2*} [a] 10^{-7} M s^{-1}	P_{1O2*} [a] µM h^{-1}	[$^1O_2$*] [b] 10^{-12} M	$f_{FFA,1O2}$ [c]	$10^2 \times \Phi_{1O2*}$ [d]
Particle Extracts					
PME1*	0.36 (0.04)	131 (15)	0.16 (0.02)	0.51 (0.08)	2.2 (0.2)
PME2*	0.68 (0.06)	246 (20)	0.31 (0.03)	0.72 (0.07)	3.8 (0.3)
PME3	2.4 (0.2)	851 (81)	1.1 (0.1)	1.1 (0.1)	5.7 (0.5)
PME4	4.2 (0.4)	1515 (135)	1.9 (0.2)	1.0 (0.1)	3.4 (0.3)
PME5	2.8 (0.2)	1000 (59)	1.3 (0.1)	1.2 (0.1)	3.8 (0.2)
PME6	4.8 (0.3)	1719 (114)	2.2 (0.1)	1.1 (0.1)	3.8 (0.3)
PME3D0.5	3.9 (0.4)	1413 (138)	1.8 (0.2)	0.79 (0.10)	4.5 (0.4)
PME3D1.3	1.1 (0.1)	414 (40)	0.52 (0.05)	0.68 (0.07)	3.6 (0.3)
PME3D2.5*	0.55 (0.03	198 (11)	0.25 (0.01)	0.61 (0.04)	3.3 (0.2)
PME3D10	0.14 (0.02)	50.8 (6.0)	0.064 (0.008)	0.59 (0.09)	3.3 (0.4)
Average (±σ)					
“Standard” (PME3-6)	3.5 (1.1)	1271 (412)	1.6 (0.5)	1.1 (0.1)	4.2 (1.0)
“Dilute” (PME1*-2*,3D2.5*)	0.53 (0.16)	192 (58)	0.24 (0.07)	0.61 (0.11)	3.1 (0.8)
Davis Fog	0.51 (0.14)	183 (49)	0.23 (0.06)	1.4 (0.8)	3.8 (3.1)
Test statistic [f]	**0.0064**	**0.0064**	**0.0064**		0.98
Field Blanks[e]					
FB1 (dilute)	≤ 0.076	≤ 27	≤ 0.0034		
FB2 (standard)	≤ 0.069	≤ 25	≤ 0.0031		

Listed uncertainties are ± 1 standard error unless otherwise stated.

All equations involved in the technique are discussed in Kaur and Anastasio (2017).

* Samples extracted in 2.5 mL/filter square and referred to as the “dilute” extracts in the main text.

[a] Davis winter solstice-normalized rate of $^1O_2$* formation.

[b] Davis winter solstice-normalized steady-state concentration of $^1O_2$*.

[c] Fraction of probe FFA lost due to $^1O_2$*.

[d] Apparent quantum yield of $^1O_2$*, calculated as $\Phi_{1O2*} = P_{1O2} / R_{abs.}$

[e] Blanks were analyzed by measuring FFA loss in undiluted blanks. This is an upper bound determined by ascribing all FFA loss to $^1O_2$*.

[f] Test statistic for comparison of standard PME and Davis fog averages: *p*-value for a two-tailed *t*-test for samples of unequal variance. Values below 0.05 are in bold.

Table S8. Syringol loss kinetics

Sample ID	k'_{SYR} [a] 10^{-5} s^{-1}	τ_{SYR} [b] h	$k'_{\mathrm{SYR,OH}}$ [c] 10^{-5} s^{-1}	$k'_{\mathrm{SYR,1O2}}$ [d] 10^{-5} s^{-1}	$k'_{\mathrm{SYR,3C*}}$ [e] 10^{-5} s^{-1}	$f_{\mathrm{SYR,3C*}}$ [f]
Particle Extracts						
PME1*	12 (1)	2.3 (0.3)	0.43 (0.04)	0.59 (0.07)	11 (1)	0.92 (0.15)
PME2*	14 (2)	2.0 (0.3)	1.2 (0.1)	1.1 (0.09)	11 (2)	0.83 (0.17)
PME3	33 (1)	0.85 (0.03)	2.1 (0.5)	3.9 (0.4)	27 (1)	0.82 (0.06)
PME4	69 (8)	0.40 (0.04)	1.6 (0.2)	6.9 (0.6)	61 (8)	0.88 (0.15)
PME5	35 (2)	0.80 (0.04)	0.74 (0.07)	4.5 (0.3)	29 (2)	0.85 (0.06)
PME6	37 (3)	0.74 (0.05)	0.85 (0.09)	7.8 (0.5)	24 (3)	0.77 (0.09)
PME3D0.5	48 (3)	0.58 (0.04)	1.9 (0.5)	6.4 (0.6)	40 (3)	0.83 (0.08)
PME3D1.3	26 (2)	1.1 (0.1)	0.78 (0.21)	1.9 (0.2)	24 (2)	0.90 (0.11)
PME3D2.5*	15 (2)	1.9 (0.3)	0.86 (0.26)	0.90 (0.05)	13 (2)	0.88 (0.19)
PME3D10	3.6 (0.4)	7.7 (0.8)	1.7 (0.7)	0.23 (0.03)	1.6 (0.8)	0.46 (0.24)
Average (±σ)						
“Standard” (PME3-6)	43 (17)	0.70 (0.20)	1.3 (0.7)	5.8 (1.9)	36 (16)	0.83 (0.05)
“Dilute” (PME1*-2*,3D2.5*)	14 (1)	2.0 (0.2)	0.82 (0.37)	0.87 (0.26)	12 (1)	0.88 (0.04)
Davis Fog	16 (11)	2.4 (1.4)	1.1 (0.2)	0.83 (0.22)	14 (11)	0.85 (0.06)
Test statistic [g]	**0.040**					
Field Blanks						
FB1 (dilute)	1.3 (0.2)	22 (3)				
FB2 (standard)	0.95 (0.07)	29 (2)				

Listed uncertainties are ± 1 standard error unless otherwise stated.

Bimolecular rate constants are given in Table S10.

* Samples extracted in 2.5 mL/filter square and referred to as the “dilute” extracts in the main text.

[a] Davis winter-solstice-normalized value of the measured pseudo-first-order rate constant for loss of syringol (SYR).

[b] Lifetime of syringol, calculated as $1/k'_{\mathrm{SYR}}$.

[c] Pseudo-first-order rate constant for loss of SYR due to hydroxyl radical, calculated as $k'_{\mathrm{SYR,OH}} = k_{\mathrm{SYR+OH}} \times [^{\bullet}\mathrm{OH}]$.

[d] Pseudo-first-order rate constant for loss of SYR due to singlet oxygen, calculated as $k'_{\mathrm{SYR,1O2}} = k_{\mathrm{SYR+1O2}} \times [^{1}\mathrm{O_2}^*]$.

[e] Pseudo-first-order rate constant for loss of SYR due to triplet excited states, calculated as $k'_{\mathrm{SYR,3C*}} = k'_{\mathrm{SYR}} - (k'_{\mathrm{SYR,OH}} + k'_{\mathrm{SYR,1O2}})$.

[f] Fraction of SYR loss due to triplets, calculated as $k'_{\mathrm{SYR,3C*}} / k'_{\mathrm{SYR}}$.

[g] Test statistic for comparison of standard PME and Davis fog averages: *p*-value for a two-tailed *t*-test for samples of unequal variance. Values below 0.05 are in bold.

Table S9. Methyl jasmonate loss kinetics

Sample ID	k'_{MeJA} [a] 10^{-5} s^{-1}	τ_{MeJA} [b] h	$k'_{\mathrm{MeJA,OH}}$ [c] 10^{-5} s^{-1}	$k'_{\mathrm{MeJA,1O2}}$ [d] 10^{-5} s^{-1}	$k'_{\mathrm{MeJA,3C*}}$ [e] 10^{-5} s^{-1}	$f_{\mathrm{MeJA,3C*}}$ [f]
Particle Extracts						
PME1*	0.98 (0.13)	28 (4)	0.11 (0.01)	0.099 (0.010)	0.77 (0.13)	0.79 (0.17)
PME2*	1.1 (0.1)	26 (1)	0.30 (0.04)	0.19 (0.02)	0.59 (0.07)	0.55 (0.07)
PME3	2.4 (0.2)	12 (1)	0.53 (0.13)	0.64 (0.06)	1.2 (0.2)	0.51 (0.10)
PME4	3.5 (0.4)	7.9 (0.8)	0.42 (0.04)	1.1 (0.1)	2.0 (0.4)	0.56 (0.12)
PME5	1.7 (0.2)	16 (2)	0.19 (0.02)	0.76 (0.04)	0.79 (0.18)	0.45 (0.11)
PME6	2.7 (0.2)	10 (1)	0.22 (0.02)	1.3 (0.1)	1.2 (0.2)	0.44 (0.08)
PME3D0.5	4.7 (0.5)	5.9 (0.7)	0.49 (0.12)	1.1 (0.1)	3.1 (0.6)	0.67 (0.14)
PME3D1.3	2.6 (0.2)	11 (1)	0.20 (0.05)	0.31 (0.03)	2.1 (0.3)	0.80 (0.12)
PME3D2.5*	1.8 (0.2)	16 (2)	0.22 (0.07)	0.15 (0.01)	1.4 (0.2)	0.79 (0.15)
PME3D10	0.67 (0.09)	42 (5)	0.44 (0.19)	0.038 (0.005)	0.19 (0.21)	0.28 (0.31)
Average (±σ)						
“Standard” (PME3-6)	2.6 (0.7)	11 (3)	0.34 (0.16)	0.96 (0.31)	1.3 (0.5)	0.49 (0.05)
“Dilute” (PME1*-2*,3D2.5*)	1.3 (0.4)	23 (7)	0.21 (0.10)	0.15 (0.04)	0.92 (0.42)	0.71 (0.14)
Davis Fog	0.90 (0.12)	31 (4)	0.28 (0.05)	0.14 (0.04)	0.48 (0.17)	0.53 (0.13)
Test statistic [g]	**0.018**					
Field Blanks						
FB1 (dilute)	0.17 (0.2)	160 (18)				
FB2 (standard)	0.27 (0.08)	104 (31)				

Listed uncertainties are ± 1 standard error unless otherwise stated.

Bimolecular rate constants are given in Table S10.

* Samples extracted in 2.5 mL/filter square and referred to as the “dilute” extracts in the main text.

[a] Davis winter-solstice-normalized measured pseudo-first-order rate constant for loss of methyl jasmonate (MeJA).

[b] Lifetime of methyl jasmonate, calculated as $1/k'_{\mathrm{MeJA}}$.

[c] Pseudo-first-order rate constant for loss of MeJA due to hydroxyl radical, calculated as $k'_{\mathrm{MeJA,OH}} = k_{\mathrm{MeJA+OH}} \times [^{\bullet}\mathrm{OH}]$.

[d] Pseudo-first-order rate constant for loss of MeJA due to singlet oxygen, calculated as $k'_{\mathrm{MeJA,1O2}} = k_{\mathrm{MeJA+1O2}} \times [^{1}\mathrm{O}_2^{*}]$.

[e] Pseudo-first-order rate constant for loss of MeJA due to triplet excited states, calculated as $k'_{\mathrm{MeJA,3C*}} = k'_{\mathrm{MeJA}} - (k'_{\mathrm{MeJA,OH}} + k'_{\mathrm{MeJA,1O2}})$.

[f] Fraction of MeJA loss due to triplets, calculated as $k'_{\mathrm{MeJA,3C*}} / k'_{\mathrm{MeJA}}$.

[g] Test statistic for comparison of standard PME and Davis fog averages: p-value for a two-tailed t-test for samples of unequal variance. Values below 0.05 are in bold.

Table S10. Second-order rate constants for reactions of syringol and methyl jasmonate with hydroxyl radical, singlet oxygen, and triplet excited states

Oxidants	$k_{\mathrm{SYR+Oxidant}}$ 10^9 $\mathrm{M^{-1}\ s^{-1}}$	Reference	$k_{\mathrm{MeJA+Oxidant}}$ 10^8 $\mathrm{M^{-1}\ s^{-1}}$	Reference	
$^{\bullet}$OH	26	O'Neill and Steenken (1977)	67 (± 3)	Richards-Henderson et al. (2014a)	
$^1O_2$*	0.0036	Tratnyek and Hoigne (1991a)	0.0060 (± 0.0007)	Richards-Henderson et al. (2014b)	
Model Triplets (^{3}C*)					$k_{\mathrm{SYR+3C*}}$/ $k_{\mathrm{MeJA+3C*}}$ [a]
^{3}2AN*	1.9 (± 0.1)	Kaur and Anastasio (2018)	0.19 (± 0.07)	Kaur and Anastasio (2018)	100 (± 37)
^{3}3MAP*	3.8 (± 0.6)	Kaur and Anastasio (2018)	1.2 (± 0.3)	Richards-Henderson et al. (2014b)	32 (± 9)
^{3}DMB*	3.5 (± 0.8)	Smith et al. (2015)	4.1 (± 1.6)	Richards-Henderson et al. (2014b)	8.5 (± 3.8)
^{3}BP*	8.5 (± 1.6)	Kaur and Anastasio (2018)	51 (± 9)	Kaur and Anastasio (2018)	1.7 (± 0.4)

Listed uncertainties are ±1 standard error.

[a] Ratio of the bimolecular rate constants for reaction of a given model triplet with syringol (SYR) and methyl jasmonate (MeJA).

Table S11. Characteristics of model triplet species

Model Triplet	E_T [a] (kJ mol^{-1})	$E^0*({}^3C*/C^{\bullet -})$ [b] (V)	k_{O2+3C*} [c] (10^9) $M^{-1}s^{-1}$	f_Δ [d]
^{3}2AN*	249	1.10	2.5	0.81 (C_6H_6)
^{3}3MAP*	303	1.64	3.3	0.33 (C_6H_6)
^{3}DMB*	298 (estimated)[e]	-	-	< 0.61 (MeOH) (estimated)[e]
^{3}BP*	288	1.67	2.6	0.35 (C_6H_6)

All values from Canonica et al.(Canonica et al., 2000) and Wilkinson et. al.(Wilkinson et al., 1993)

[a] Triplet state energy ($T_1 \rightarrow S_0$).

[b] One-electron reduction potential for the triplet/triplet radical anion pair.

[c] Bimolecular rate constant for quenching of triplet by molecular O_2. To calculate rates of triplet photoformation (described in the main text), an average value of 2.8 (± 0.4) × 10^9 $M^{-1}s^{-1}$ is used.

[d] Yield of singlet oxygen from quenching of model triplet species by O_2. The solvent used in the determination is indicated in parentheses. Including the upper-bound value of 0.61 for ^{3}DMB* (discussed in footnote *e*), the average value of f_Δ for the model triplets is 0.53 (± 0.23).

[e] Since the E_T and f_Δ values for ^{3}DMB* are not available, values for benzaldehyde (Hunter, 1970; Wilkinson et al., 1993) are used as estimates. The f_Δ value is an upper-bound estimate.

Table S12. Best triplet matches and best estimate triplet steady-state concentrations

		Mole-fractions of Best Triplet Matches [b]				Bimolecular rate constants (M^{-1} s^{-1}) $\chi_{3C1*} \times k_{Probe+3C1*} + \chi_{3C2*} \times k_{Probe+3C2*}$ [c]			Triplet Steady-State Concentration (10^{-14} M)		
Sample ID	$k'_{SYR,3C*}$ / $k'_{MeJA,3C*}$ [a]	^{3}2AN*	^{3}3MAP*	^{3}DMB*	^{3}BP*	SYR	MeJA	SYR/MeJA Ratio	$\sum[^{3}C_{i}*]_{SYR}$ [d]	$\sum[^{3}C_{i}*]_{MeJA}$ [e]	$\sum[^{3}C_{i}*]$ (± 1S.E.) Best Estimate [f,g]
PME1*	15 (3)		0.55	0.45		3.7E+09	2.5E+08	15	3.1	3.1	3.1 (1.2)
PME2*	20 (4)		0.76	0.24		3.7E+09	1.9E+08	20	3.1	3.1	3.1 (1.0)
PME3	20 (4)		0.77	0.23		3.7E+09	1.9E+08	20	7.3	7.3	7.3 (2.3)
PME4	30 (7)		0.98	0.02		3.8E+09	1.3E+08	30	16	16	16 (5)
PME5	37 (8)	0.34	0.66			3.2E+09	8.5E+07	37	9.3	9.3	9.3 (3.1)
PME6	24 (4)		0.86	0.14		3.8E+09	1.6E+08	24	7.7	7.7	7.7 (2.2)
PME3D0.5	12 (2)		0.41	0.59		3.6E+09	2.9E+08	12	11	11	11 (5)
PME3D1.3	12 (2)		0.38	0.62		3.6E+09	3.0E+08	12	6.3	6.3	6.3 (2.6)
PME3D2.5*	10 (3)		0.22	0.78		3.6E+09	3.5E+08	10	3.5	3.5	3.5 (1.7)
PME3D10	7.9 (7.6)			0.99	0.01	3.5E+09	4.5E+08	7.9	0.51	0.51	0.51 (0.36)

Uncertainties in parentheses are ± 1 standard error.

Details of the technique are discussed in Kaur and Anastasio (2018).

* Samples extracted in 2.5 mL/filter square and referred to as the “dilute” extracts in the main text.

[a] Ratio of measured values of $k'_{Probe,3C*}$ in a given particle extract

[b] Mole fractions of model triplets whose $k_{Probe+3C*Model}$ ratio lies closest to the $k'_{Probe,3C*}$ ratio in each sample.

[c] Mole-fraction-weighted bimolecular rate constants for both probes.

[d] Triplet steady-state concentration calculated from syringol loss as $k'_{SYR,3C*} / (\chi_{3C1*}\ k_{SYR+3C1*} + \chi_{3C2*} \times k_{SYR+3C2*})$

[e] Triplet steady-state concentration calculated from methyl jasmonate loss as $k'_{MeJA,3C*} / (\chi_{3C1*} \times k_{MeJA+3C1*} + \chi_{3C2*} \times k_{MeJA+3C2*})$

[f] Best estimate steady-state concentration calculated as the average of the $\Sigma[^{3}C_{i}*]_{SYR}$ and $\Sigma[^{3}C_{i}*]_{MeJA}$.

[g] Uncertainties in parentheses are ± 1 SE propagated from the errors of $k'_{SYR,3C*}$ and $k'_{MeJA,3C*}$ and the mole-fraction-weighted bimolecular rate constants. Values are shown in Tables S8 and S9.

Table S13. Measurements of triplet excited states of organic matter

Sample ID	$\sum[^3C_i*]$ Best Estimate [a] 10^{-14} M	P_{3C*} [b] 10^{-7} M s^{-1}	P_{3C*} [b] µM h^{-1}	$10^2 \times \Phi_{3C*}$ [c]	$\frac{\Phi_{3C^*}}{(\Phi_{1O2^*}/f_{\Delta})}$ [d] *	$\frac{\Sigma[^3C_i^*]}{[^1O_2^*]}$ [e]
Particle Extracts						
PME1*	3.1 (1.2)	0.30 (0.13)	109 (48)	1.8 (0.8)	0.44 (0.20)	0.19 (0.07)
PME2*	3.1 (1.0)	0.34 (0.13)	122 (47)	1.9 (0.7)	0.26 (0.10)	0.10 (0.03)
PME3	7.3 (2.3)	1.5 (0.6)	534 (204)	3.6 (1.4)	0.33 (0.13)	0.068 (0.022)
PME4	16 (5)	3.5 (1.4)	1260 (501)	2.8 (1.1)	0.44 (0.18)	0.083 (0.029)
PME5	9.3 (3.1)	1.5 (0.6)	534 (211)	2.0 (0.8)	0.28 (0.11)	0.074 (0.025)
PME6	7.7 (2.2)	1.6 (0.6)	568 (206)	1.3 (0.5)	0.18 (0.06)	0.035 (0.011)
PME3D0.5	11 (5)	3.6 (1.6)	1286 (593)	4.1 (1.9)	0.48 (0.23)	0.062 (0.026)
PME3D1.3	6.3 (2.6)	1.1 (0.5)	393 (182)	3.4 (1.6)	0.50 (0.24)	0.12 (0.05)
PME3D2.5*	3.5 (1.7)	0.44 (0.24)	160 (86)	2.7 (1.5)	0.43 (0.23)	0.14 (0.07)
PME3D10	0.51 (0.36)	0.0047 (0.0034)	17 (12)	1.1 (0.8)	0.18 (0.13)	0.079 (0.057)
Averages (±σ)						
"Standard" (PME3-6)	10 (4)	2.0 (1.0)	723 (355)	2.4 (1.0)	0.31 (0.11)	0.065 (0.021)
"Dilute" (PME1*-2*,3D2.5*)	3.2 (0.2)	0.36 (0.01)	130 (26)	2.1 (0.5)	0.38 (0.10)	0.14 (0.04)
Davis Fog	5.4 (6.3)	0.59 (0.60)	212 (216)	5.8 (8.6)	0.55 (0.44)	0.21 (0.20)
Test statistic [f]	0.27	**0.059**	**0.059**	0.49	0.35	0.25

Listed uncertainties are ± 1 standard error.

* Samples extracted in 2.5 mL/filter square and referred to as the "dilute" extracts in the main text.

[a] Best estimate of oxidizing triplets steady-state concentration, calculated as the average of the $\Sigma[^3C_i*]_{SYR}$ and $\Sigma[^3C_i*]_{MeJA}$ values, as shown in Table S12.

[b] Davis winter solstice-normalized rate of triplet photoproduction, calculated as $P_{3C*} = \Sigma[^3C_i*] \times (k_{3C*+O2} \times [O_2] + \mathbf{(}k_{rxn} + k_Q\mathbf{)}[DOC]\mathbf{)}$) (Eq. (8), main text).

[c] Quantum yield for formation of oxidizing organic triplet excited states, calculated as $\Phi_{3C*} = P_{3C*} / R_{abs}$.

[d] Fraction of the total triplet pool that can oxidize our probes, i.e., that are "oxidizing triplets". This is estimated as the ratio of the quantum yields for oxidizing triplets and singlet oxygen (Table S7) divided by the average yield of $^1O_2$* ($f_\Delta = 0.53$; Table S11) from ^3C* via energy transfer. The denominator, Φ_{1O2}/f_Δ , is an estimate of the quantum yield for formation of energy-transfer triplets that can make singlet molecular oxygen, a pool that likely includes essentially all organic triplet states.

[e] Ratio of the Davis-winter-normalized steady-state triplet and singlet oxygen concentrations.

[f] Test statistic for comparison of standard PME and Davis fog averages: *p*-value for a two-tailed *t*-test for samples of unequal variance. Values below 0.05 are in bold.

Table S14. Particle mass to water mass ratios in the PME3 extracts, typical fog drops, and particles

Sample ID	Number of filter squares extracted	Volume of Milli-Q water per filter square (mL) [a]	Aqueous PM mass concentration factor (CF) [b]	Average PM mass extracted per filter square (µg) [c]	Total PM mass extracted (µg) [d]	Total volume of extract (mL) [e]	PM mass / water mass (µg-PM / µg-H_2O) [f]
PME3D10	1	10	0.05	347	347	10	3.5E-05
PME3D2.5	12	2.5	0.20	331 (15)	3977	30	1.3E-04
PME3D1.3	8	1.3	0.38	315 (23)	2520	10	2.4E-04
PME3D1 or "PME3"	12	1.0	0.49	328 (19)	3932	12	3.3E-04
PME3D0.5	26	0.5	0.96	323 (21)	10979	13	8.4E-04
Cloud/Fog drop							(1 – 5)E-04 [g]
Particles							≥ 1 [h]

[a] Volume of water used to extract each 2 × 2 cm square piece of the filter sheet.

[b] PM mass concentration factor in the extract (Eq. (10), main text).

[c] Average (± 1σ) mass extracted from the filter squares for each dilution.

[d] Total mass extracted per extract. For each extract, the filter pieces used in the extraction were weighed pre- and post-extraction using a Mettler Toledo XP2U ultra-microbalance (error ± 2 µg). The PM mass extracted is the difference between pre- and post-extraction weights.

[e] Total volume of extract = number of filter pieces extracted × water volume per filter square.

[f] PM mass-to-water mass ratio, calculated as total solute mass extracted / total volume of extract.

[g] For fog drops , we estimate that PM mass/water mass ratios are in the range of $(1 – 5) \times 10^{-4}$ µg-PM/µg-H_2O based on a typical PM mass of 31 µg m^3-air in California's Central Valley, as measured by Young et al. (2016), and assuming a range for the liquid water content (LWC) of 0.06 to 0.3 g-H_2O m^{-3}-air (Hess et al., 1998).

[h] Based on measurements of particle mass concentration (Young et al. (2016)) and estimated particle water (Parworth et al., 2017) in California's Central Valley during winter, the calculated range of PM mass to water mass ratios is 0.79 – 50. From this range, we use a value of 1 to represent typical PM conditions.

Table S15. Photooxidant concentrations (formed *in situ*) in PME3D extracts and expected values in ambient particles

Sample ID	Aqueous PM Mass Concentration Factor (CF) [a]	PM Mass /Water Mass (µg-PM/µg-H_2O) [b]	[$^{\bullet}$OH] (M)	[$^1O_2$*] (M)	∑[^3C_i*] (M)
PME3D10	0.05	3.5E-05	6.7E-16	6.4E-14	5.1E-15
PME3D2.5*	0.20	1.3E-04	3.4E-16	2.5E-13	3.5E-14
PME3D1.3	0.38	2.4E-04	3.2E-16	5.2E-13	6.3E-14
PME3D1	0.49	3.3E-04	8.5E-16	1.1E-12	7.3E-14
PME3D0.5	0.96	8.4E-04	8.3E-16	1.8E-12	1.1E-13
Ambient Particles		1.0	8.4E-16 [c]	1.6E-10 [d]	2.3E-13 [e] 1.3E-11 [f]

[a] Aqueous PM mass concentration factor (Eq. (10), main text).

[b] PM mass/water mass ratio (Table S14).

[c] Expected *in situ* [$^{\bullet}$OH] concentration in ambient PM (in the absence of partitioning of $^{\bullet}$OH from the gas phase), determined as the average of the five measurements in PME3D extracts and corrected for quenching by probe MBO (Sect. S1.1). Including mass transport of $^{\bullet}$OH(g) to the drops will increase the aqueous concentration by approximately 30%, as discussed in the text.

[d] Expected [$^1O_2$*] concentration in ambient PM; see section S4..

[e] Best estimate for the ∑[^3C_i*] concentration in ambient PM, obtained by plotting ∑[^3C_i*] against the PM mass/water mass ratio, fitting the data to the equation $y = ax/(1+bx)$; parameters $a = 3.08 \times 10^{-10}$ M and $b = 1.31 \times 10^3$ were obtained using Excel. The curve was then extrapolated to a PM mass/water mass ratio of 1.0 µg-PM/µg-H_2O.

[f] High estimate for the ∑[^3C_i*] concentration in ambient PM, obtained by fitting ∑[^3C_i*] against PM mass/water mass ratio with the equation $y = ax/(1+bx)$; parameters $a = 2.26 \times 10^{-10}$ M and $b = 17.0$ were obtained using Excel. The curve was then extrapolated to a PM mass/water mass ratio of 1.0 µg-PM/µg-H_2O.

Table S16. Gas- and aqueous-phase reaction rate constants for selected organic compounds with the major oxidants

#	Organic Compound	Gas-phase rate constant, $k_{ORG+Ox(g)}$ (cm^3 mlc^{-1} s^{-1})				Aqueous-phase rate constants, $k_{ORG+Ox(aq)}$ (M^{-1} s^{-1})							
		$^{\bullet}$OH(g)	Ref.	O_3(g)	Ref.	$^{\bullet}$OH(aq)	Ref.	$^{1}O_2$*(aq)	Ref.	O_3(aq)	Ref.	^{3}C*(aq) [a]	Ref.
1	Syringol	9.6E-11	(Lauraguais et al., 2012)	4.0E-19 [b]	(Zein et al., 2015)	2.6E+10	(O'Neill and Steenken, 1977)	3.6E+07	(Tratnyek and Hoigne, 1991b)	1.3E+04 [c]	(Hoigné and Bader, 1983)	3.7E+09	(Kaur and Anastasio, 2018), (Smith et al., 2015)
2	Methyl jasmonate	7.8E-12 [d]	(Meylan and Howard, 1993)	1.7E-16 [d]	(Meylan and Howard, 1993)	6.7E+09	(Richards-Henderson et al., 2014a)	6.0E+06	(Richards-Henderson et al., 2014b)	1.0E+05 [e]	(Richards-Henderson et al., 2014b)	2.7E+08	(Kaur and Anastasio, 2018)
3	Tyrosine	2.8E-11 [f]	(Rinke and Zetzsch, 1984)	4.7E-19 [g]	(Atkinson et al., 1982)	1.3E+10	(Solar et al., 1984)	3.8E+07	(Bertolotti et al., 1991)	3.3E+05 (pH 4.2)	(McGregor and Anastasio, 2001)	6.6E+08 [h]	(Canonica et al., 2000)
4	1,2,4-Butanetriol	8.5E-12 [i]	(Atkinson et al., 2006)	1.0E-20 [j]	(Atkinson et al., 2006)	5.0E+09 [k]	(Anbar et al., 1966)	6.0E+04 [l]	(Wilkinson et al., 1995)	2 [m]	(Hoigné and Bader, 1983)	1.1E+06 [n]	(Tetreau et al., 1972)
5	3-Hydroxy-2,5-bis(hydroxymethyl) furan	4.0E-11 [o]	(Atkinson et al., 1983)	2.4E-18 [o]	(Atkinson et al., 1983)	3.9E+09 [p]	(Lilie, 1971)	1.0E+08 [q]	(Wilkinson et al., 1995)	1.2E+03 [r]	(Andreev, 2012)	1.4E+08 [s]	(Kaur and Anastasio, 2018)

References for the measured rate constants are indicated. Values indicated are at 298 K wherever available. In cases where no measurements were found, rate constants for structurally similar compounds are used as proxies; references for those are provided, and discussed in the following footnotes.

[a] For triplets, we use an average of rate constants for ^{3}3MAP* and ^{3}DMB*.

[b] Second-order rate constant for the gas-phase reaction of O_3 with guaiacol (2-methoxyphenol).

[c] Second-order rate constant for the aqueous reaction of $O_3$with phenol is used as a proxy, with a ten-fold enhancement based on the measured ratio of phenol and syringol rate constants for reaction with ^{3}DMB* (discussed in the SI of Kaur and Anastasio (2018)).

[d] Average of cis- and trans-methyl jasmonate rate constants with hydroxyl radical and ozone.

[e] Estimated by Richards-Henderson et al. (2014b) using a structurally similar compound.

[f] Second-order rate constant for the aqueous-phase reaction of O_3 with phenol.

[g] Second-order rate constant for the aqueous-phase reaction of O_3 with 3-methylphenol.

[h] Second-order rate constant for aqueous-phase reaction of tyrosine with 3'-methoxyacetophenone.

[i] Second-order rate constant for gas-phase reaction of $^{\bullet}$OH with 1-butanol.

[j] Second-order rate constant for gas-phase reaction of O_3 with pinonaldehyde.

[k] Second-order rate constant for aqueous-phase reaction of $^{\bullet}$OH with 1,6-hexanediol.

[l] Second-order rate constant for aqueous-phase reaction of $^{1}O_2$* with 2-butanol.

[m] Second-order rate constant for aqueous-phase reaction of O_3 with 2-propanol.

[n] Second-order rate constant for aqueous-phase reaction of ^{3}DMB* with 2-propanol.

[o] Second-order rate constant for gas-phase reaction of $^{\bullet}$OH and O_3 with furan.

[p] Second-order rate constant for aqueous-phase reaction of $^{\bullet}$OH with furan.

[q] Second-order rate constant for aqueous-phase reaction of $^{1}O_2$* with furan, adjusted by multiplying with 0.5 based on effect of changing substituents.

[r] Second-order rate constant for aqueous-phase reaction of O_3 with furan in glacial acetic acid.

[s] Average of the second-order rate constant for aqueous-phase reaction of ^{3}3MAP* and ^{3}DMB* with methyl jasmonate is used a proxy, adjusted by multiplying with 0.5 based on effect of changing substituents observed for rate constant of furan with $^{1}O_2$*.

Table S17. Fate of selected organic compounds in fog and particles

#	Organic Compound	K_H [a] (M atm^{-1})	f_{aq} [b]	Overall		Percent of loss due to each oxidant [e]					
				k'_{ORG} [c] (s^{-1})	τ_{ORG} [d] (h)	$^{\bullet}$OH(g)	O_3(g)	$^{\bullet}$OH(aq)	$^1O_2$*(aq)	O_3(aq)	^3C*(aq)
Fog											
1	Syringol	5.0E+03	0.11	1.1E-04	2.5	76	0	5	1	0	18
2	Methyl jasmonate	8.1E+03	0.17	1.2E-04	2.3	5	86	2	0	5	2
3	Tyrosine	8.0E+10	1.0	1.8E-04	1.6	0	0	15	4	62	19
4	1,2,4-Butanetriol	4.7E+11	1.0	1.0E-05	28	0	0	99	0	0	0
5	3-Hydroxy-2,5-bis(hydroxymethyl) furan	1.1E+09	1.0	3.5E-05	7.9	0	0	22	57	1	19
PM (Best-fit [^3C*] scenario)											
1	Syringol	5.0E+03	2.4E-06	9.6E-05	2.9	100	0	0	0	0	0
2	Methyl jasmonate	8.1E+03	4.0E-06	1.3E-04	2.1	6	94	0	0	0	0
3	Tyrosine	8.0E+10	0.98	6.3E-03	0.044	0	0	0	96	2	2
4	1,2,4-Butanetriol	4.7E+11	1.0	1.4E-05	20	0	0	30	68	0	2
5	3-Hydroxy-2,5-bis(hydroxymethyl) furan	1.1E+09	0.35	5.7E-03	0.049	0.5	0	0	99	0.0	0.2
PM (High estimate [^3C*] scenario)											
1	Syringol	5.0E+03	2.4E-06	9.6E-05	2.9	98	0	0	0	0	1
2	Methyl jasmonate	8.1E+03	4.0E-06	1.3E-04	2.1	6	94	0	0	0	0
3	Tyrosine	8.0E+10	0.98	1.4E-02	0.020	0	0	0	42	1	57
4	1,2,4-Butanetriol	4.7E+11	1.0	2.6E-05	10.5	0	0	16	37	0	47
5	3-Hydroxy-2,5-bis(hydroxymethyl) furan	1.1E+09	0.35	6.3E-03	0.044	0.4	0	0	90	0	9

For fog, a liquid water content of 1×10^{-6} L-aq / L-air is assumed.

For PM, a liquid water content of 2×10^{-11} L-aq / L-air is assumed, based on typical wintertime Central Valley conditions (Parworth et al., 2017).

[a] Henry's law constant estimated using EPISuite version 4.11(USEPA, 2012). For methyl jasmonate, measured value from Vempati (2014).

[b] Fraction of organic compound present in the aqueous-phase, calculated as $f_{aq} = 1/(1+1/(K_H \times L \times R \times T))$, where K_H is the Henry's law constant, L is the liquid water content, R is the gas constant (0.082 L atm K^{-1} mol^{-1}), and T = 298 K.

[c] Total pseudo-first order rate constant for loss of organic compound, calculated as $k'_{ORG} = \Sigma(f_{aq} \times k'_{ORG,Ox(aq)} + (1- f_{aq}) \times k'_{ORG,Ox(g)})$. $k'_{ORG,Ox(g)}$ and $k'_{ORG,Ox(aq)}$ are by calculated by multiplying the bimolecular reaction rate constant (Table S16) with the corresponding steady-state concentration of oxidant: $[^{\bullet}OH(g)] = 1 \times 10^6$ molecules cm^{-3}, $[O_3(g)]$ = 30 ppbv = 7.4×10^{11} molecules cm^{-3}, $[^{\bullet}OH(aq)] = 2 \times 10^{-15}$ M (includes gas-to-aqueous partitioning; Kaur and Anastasio (2017) and this study), $[O_3(aq)] = 3.3 \times 10^{-10}$ M (based on equilibrium with 30 ppbv O_3(g) and $K_H = 1.1 \times 10^{-2}$ M atm^{-1}; Seinfeld and Pandis (2012)), $[^1O_2*(aq)] = 2 \times 10^{-13}$ M in fog (average in Davis fog; Kaur and Anastasio (2017)), and 1.5×10^{-10} M in PM (estimate in PM after accounting for evaporative loss and loss due to organic sinks at higher DOC concentrations; Sect. S5). In case of the triplets, in fog $[^3C*(aq)] = 5 \times 10^{-14}$ M (average in Davis fog; Kaur and Anastasio (2018)); in PM both the best-fit and high-estimate concentrations obtained via extrapolation (Table S15) are considered, i.e., $[^3C*(aq)] = 2.3 \times 10^{-13}$ M and 1.3×10^{-11} M, respectively.

[d] Overall lifetime of organic compound, calculated as $1/k'_{ORG}$.

[e] Percent of organic compound lost due to each pathway, calculated as $(f_{aq} \times k'_{ORG,Ox(aq)})/k'_{ORG}$ for aqueous pathways and $((1-f_{aq}) \times k'_{ORG,Ox(g)})/k'_{ORG}$ for gas-phase processes. The sum of all pathways for a given compound is sometimes not equal to 100% because of rounding.

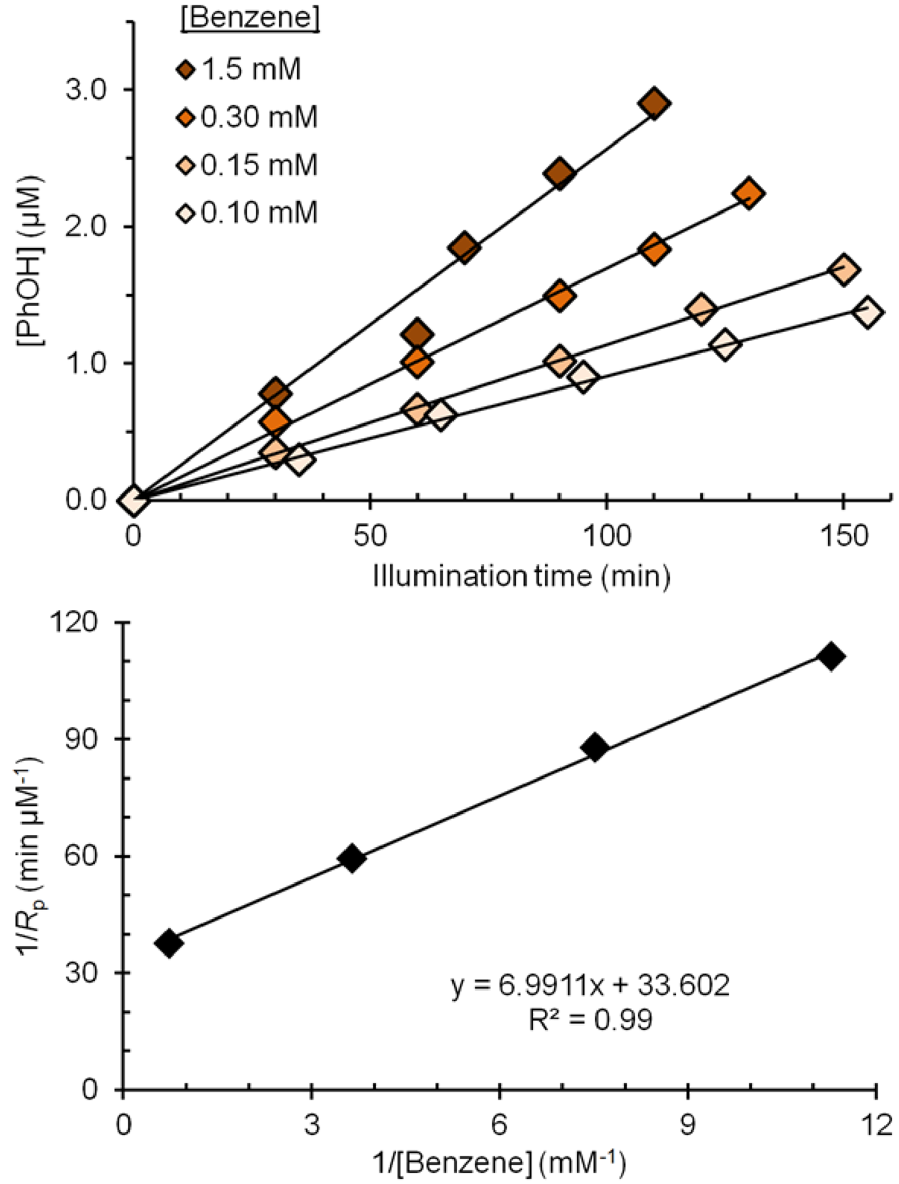

Figure S1. $^{\bullet}$OH measurement in extract PME5. Top Panel: Photoformation of phenol in four aliquots of the extract spiked with varying benzene concentrations (0.10 to 1.5 mM). The rates of phenol formation, R_p, were determined as the slopes of the linear fits for each of the four data sets. Bottom: "Inverse" plot, i.e., the inverse of R_p vs. the inverse of the benzene concentration. The slope and y-intercept from this plot are used to calculate P_{OH}, [$^{\bullet}$OH], and k'_{OH} using equations described in Kaur and Anastasio (2017). $^{\bullet}$OH results for all particle extracts are tabulated in Table S3.

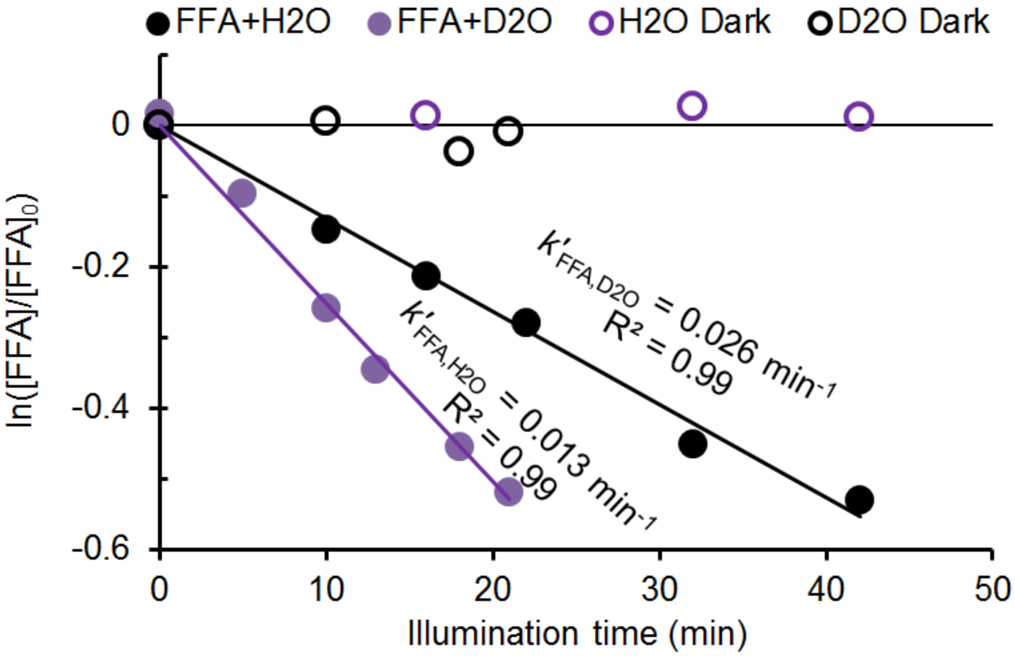

Figure S2. Singlet oxygen kinetic measurements in extract PME5 diluted 1:1 (volume : volume) with H_2O or D_2O. Data show the change in probe concentration (furfuryl alcohol, FFA) with illumination time. Closed symbols are illuminated samples while open symbols represent dark controls. Equations for calculating $^1O_2*$ steady-state concentrations and rates of photoproduction are described in Kaur and Anastasio (2017).

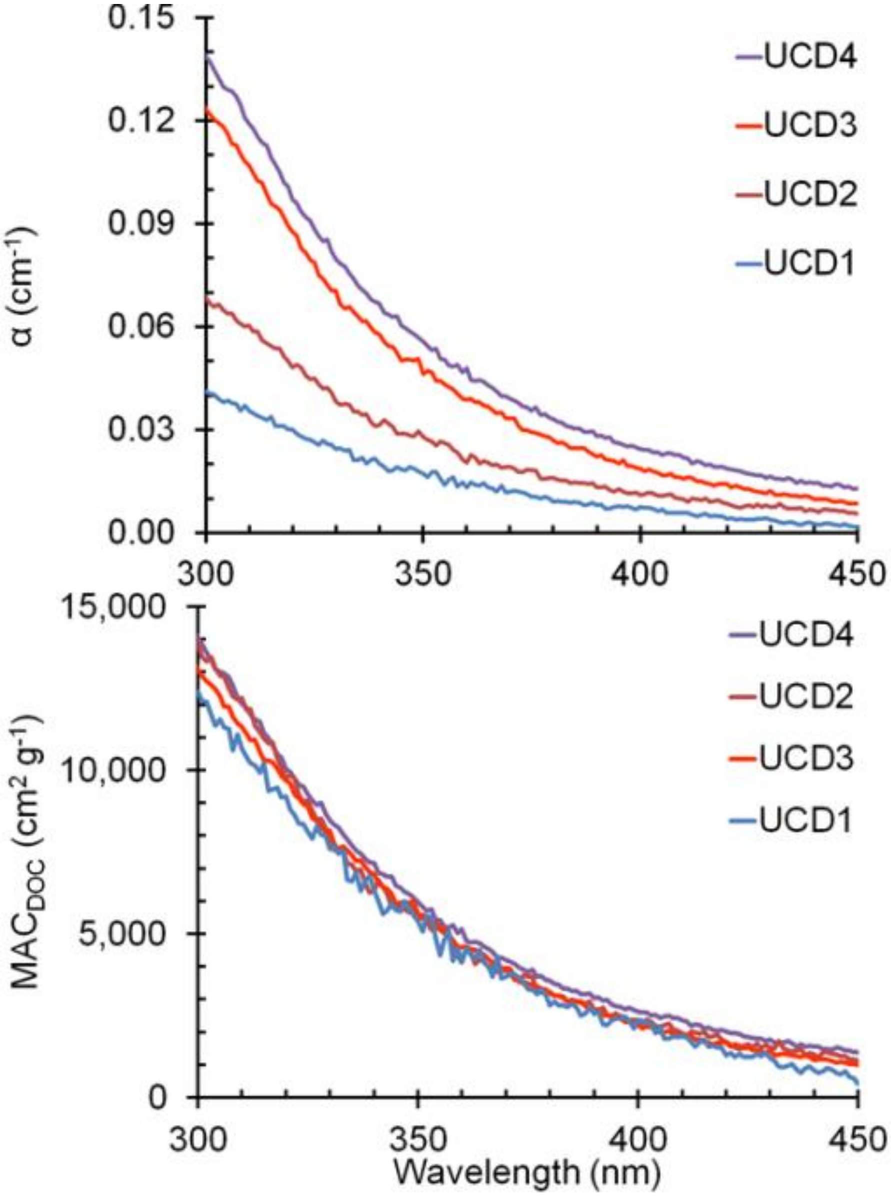

Figure S3. Top panel: Light absorbance by fog samples collected during 2011-12 in Davis, CA. The legend shows the sample identities, arranged from the highest absorbing (top) to lowest absorbing (bottom) at 300 nm. Bottom panel: Mass absorption coefficient of DOC in the Davis fog samples. All data from Kaur and Anastasio (2017).

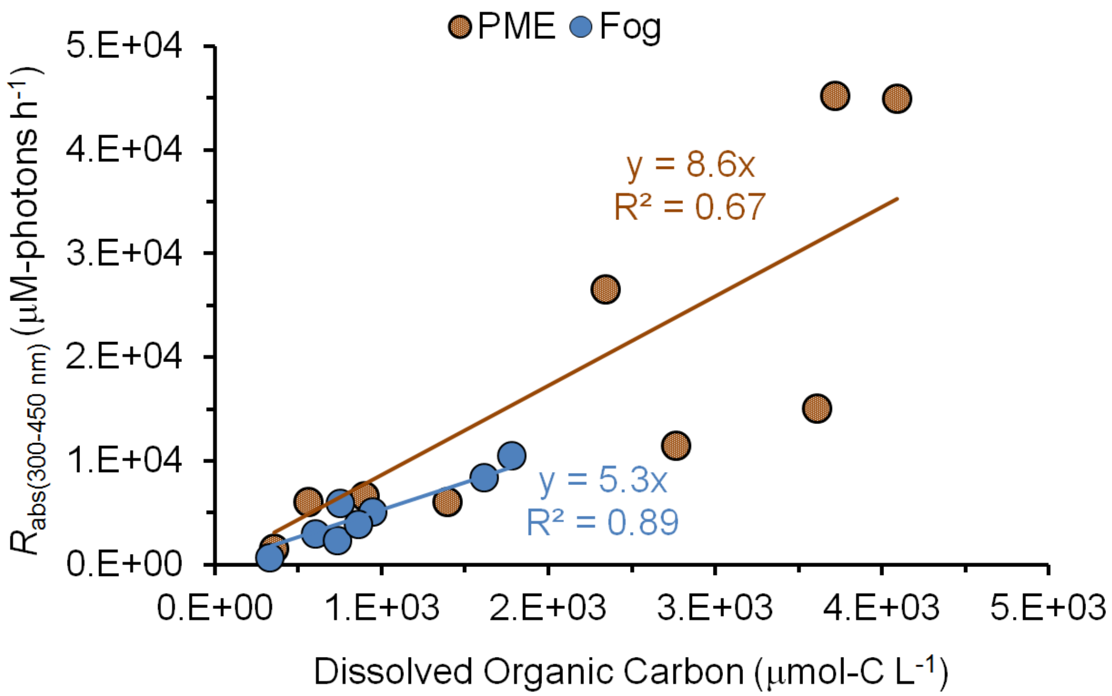

Figure S4. Correlation between the rate of sunlight absorption (R_{abs}) in the 300-450 nm wavelength range and dissolved organic carbon (DOC) for the fog samples (data from Kaur and Anastasio (2017)) and particle extracts (PME) (this work). Values for PME in this plot are summarized in Table S1.

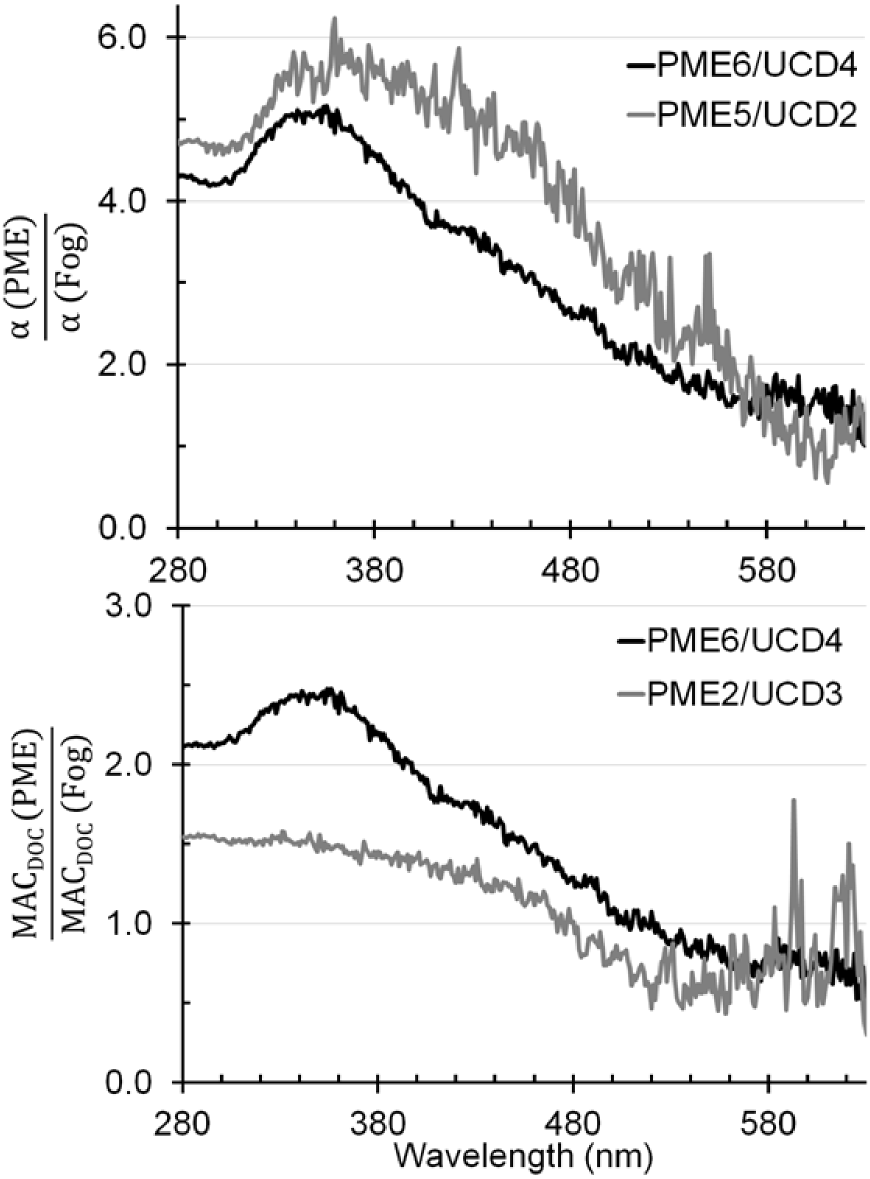

Figure S5. (Top) Ratio of pathlength-normalized absorbance for PME and fog samples with highest (black) and median (grey) absorbances. (Bottom): Ratio of mass absorption coefficients of DOC in PME and fog samples with highest (black) and median (grey) absorbances.

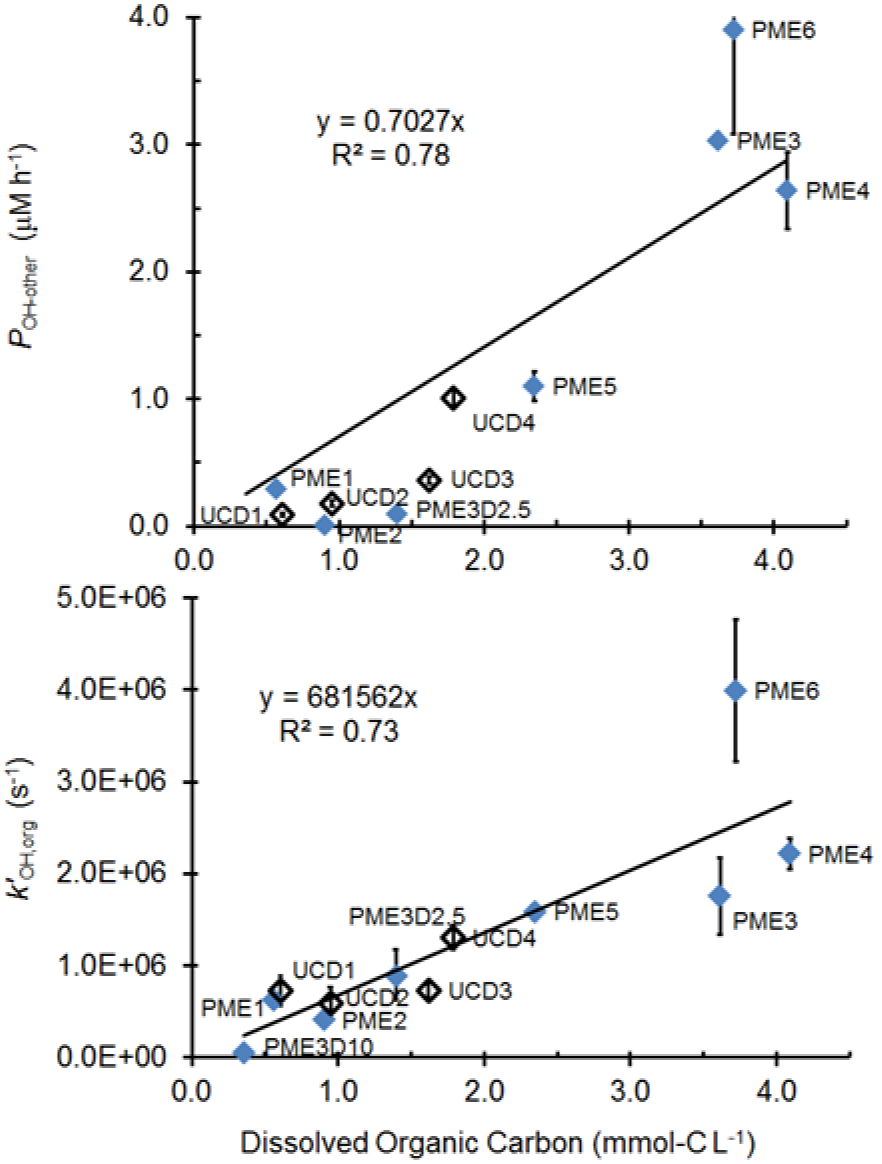

Figure S6. (Top) Correlation between the rate of $^{\bullet}$OH photoproduction due to sources other than nitrite and nitrate and the concentration of dissolved organic carbon (DOC). While the R^2 value for this correlation is relatively high, this is largely driven by the highest three points: most of the data are poorly fit by the regression line. (Bottom) Correlation between apparent pseudo-first order rate constant for loss of $^{\bullet}$OH due to organic sinks (obtained by subtracting inorganic contributions from the measured k'_{OH}) and DOC. Data include measurements in particle extracts (measured in this work) and in Davis fogs (Kaur and Anastasio, 2017).

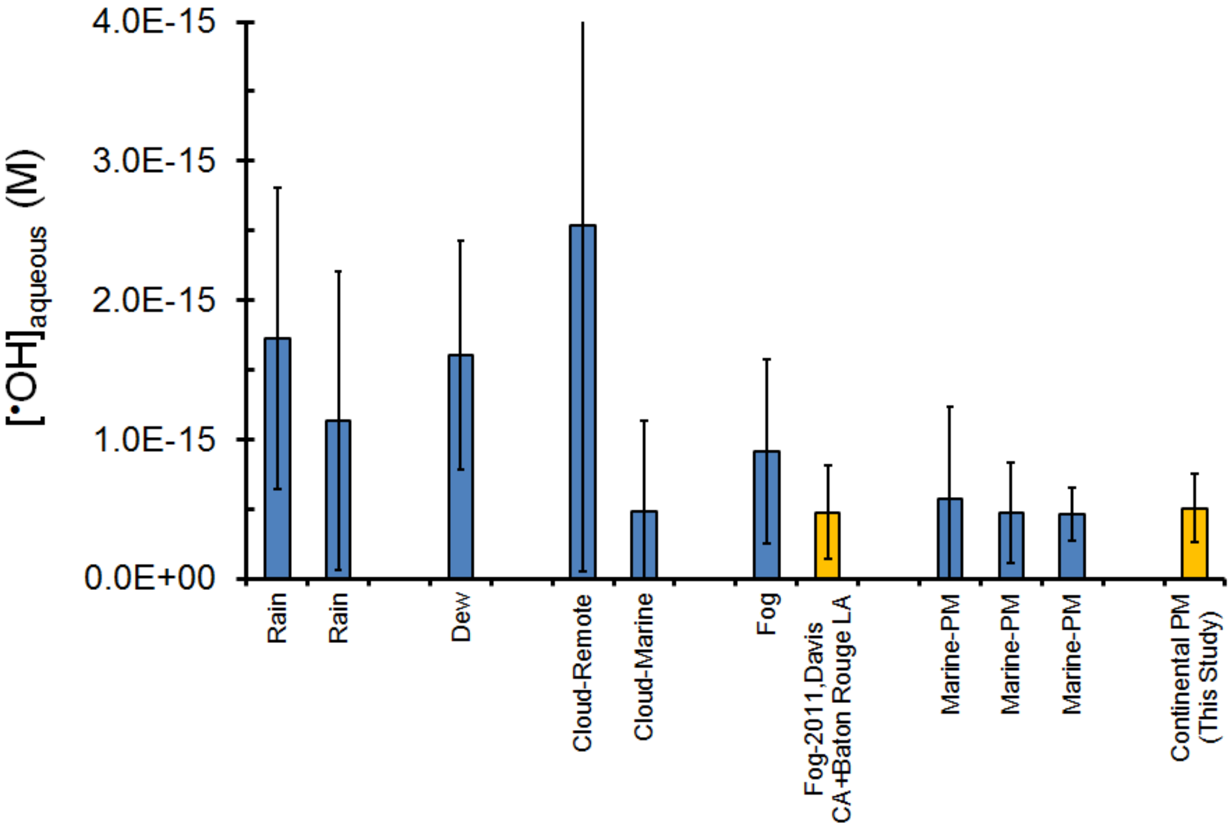

Figure S7. Comparison of hydroxyl radical steady-state concentrations formed *in situ* (i.e., not including mass transport of $^{\bullet}OH$ from the gas phase) measured in various atmospheric waters, as summarized in Arakaki et al. (2013) (blue bars) and including (in yellow bars) our recent data for fog (Kaur and Anastasio, 2017) and current data for PM. Error bars are ± 1σ, calculated from the variability in values used to calculate the mean for a given study.

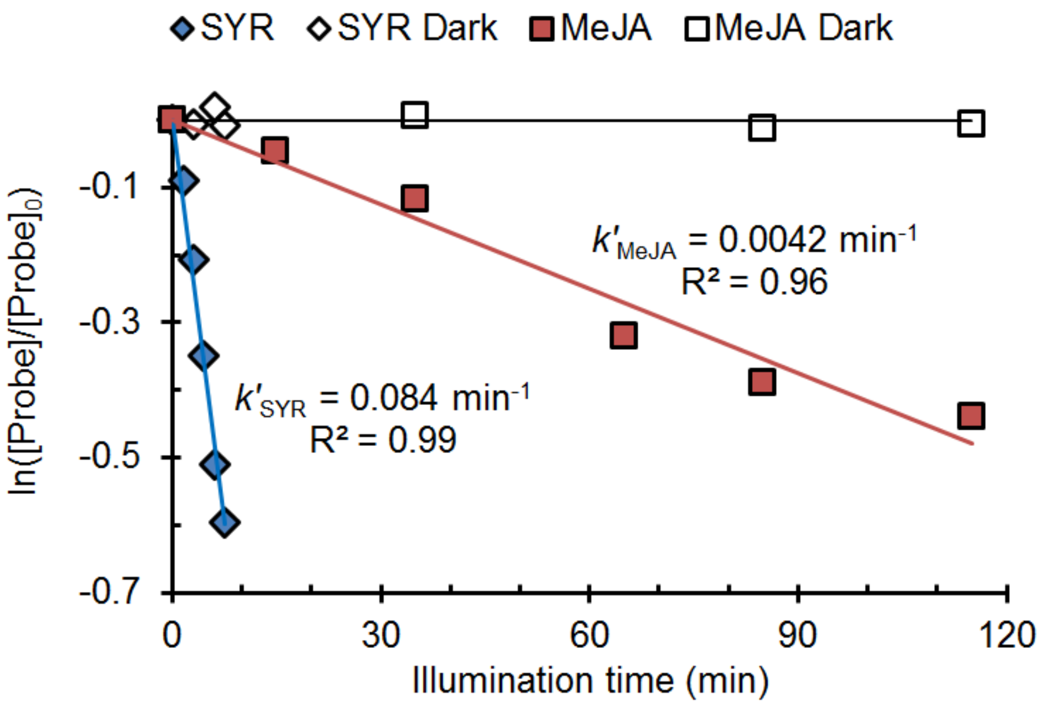

Figure S8. Loss of probes for measuring triplet excited states: syringol (SYR) and methyl jasmonate (MeJA) in extract PME5. Closed symbols are illuminated samples while open symbols represent dark controls.

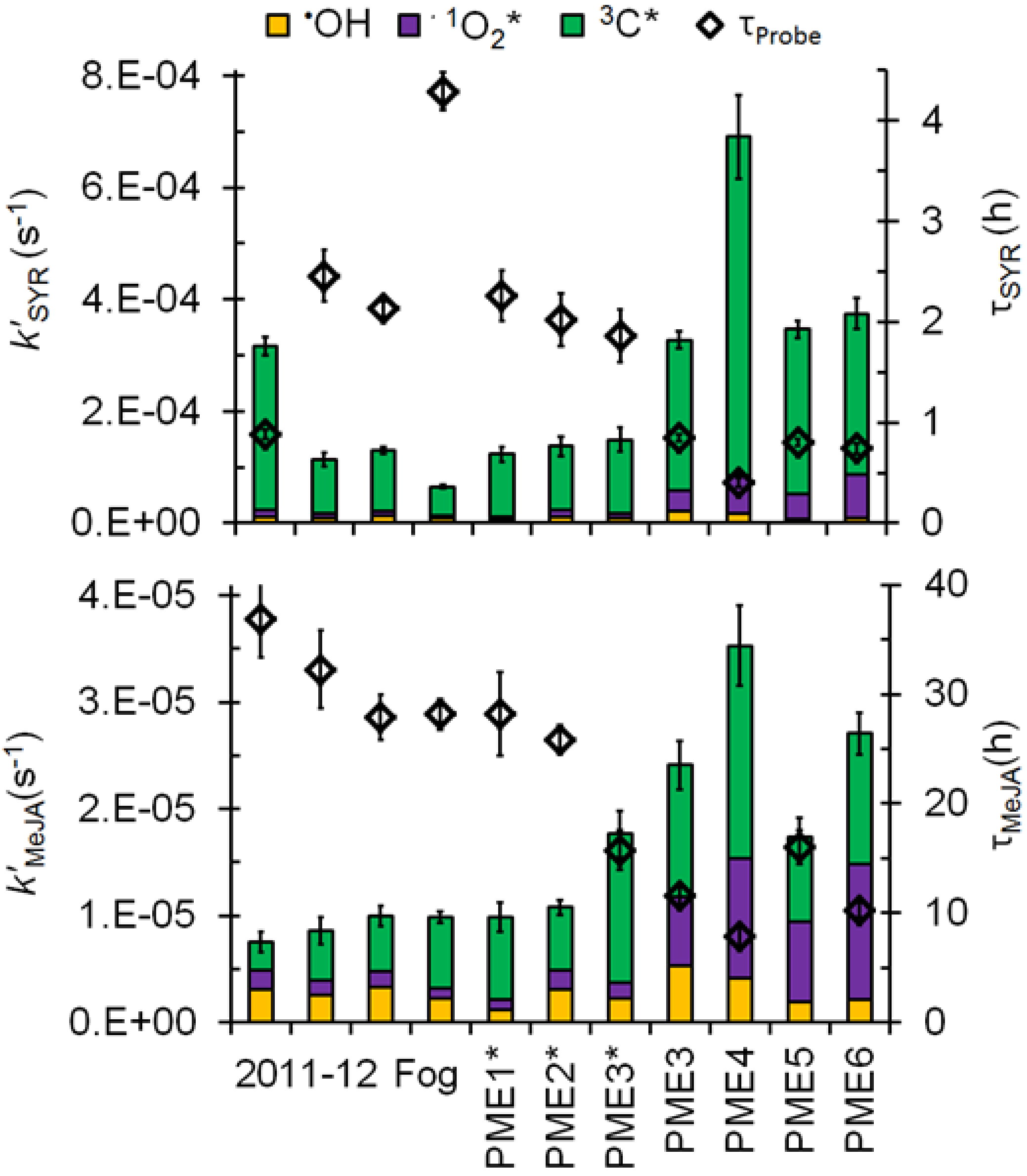

Figure S9. Winter-solstice-normalized pseudo-first-order rate constants (k'_{Probe}) for loss of syringol (top panel) and methyl jasmonate (bottom panel). The bar representing each rate constant is colored to represent the contributions of hydroxyl radical (yellow), singlet molecular oxygen (purple) and triplet excited states (green) to probe loss. The Davis winter-solstice lifetime of each probe (τ_{Probe}, black diamonds) is shown on the right y-axes. The first four bars represent probe data from wintertime fog waters collected in Davis (Kaur and Anastasio, 2018)

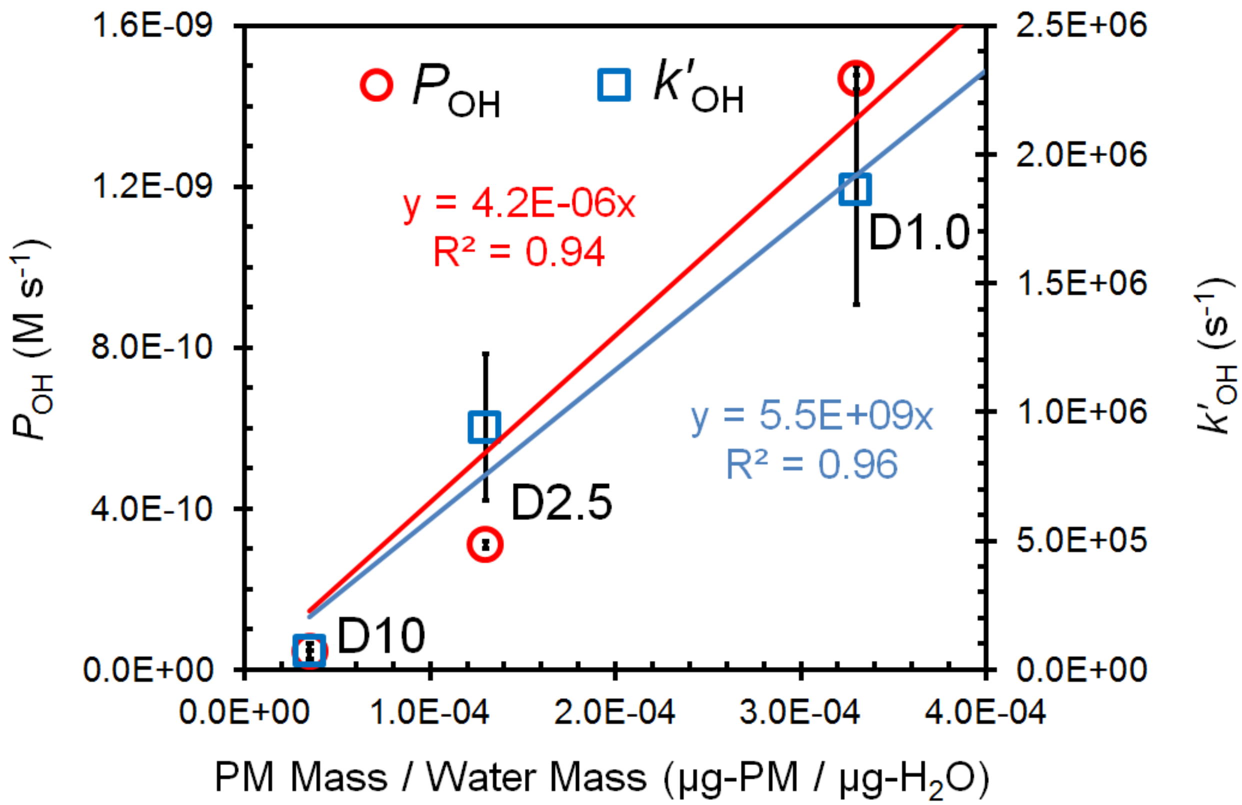

Figure S10. Dependence of rate of $^{\bullet}$OH photoproduction (P_{OH}; red circles, left y-axis) and rate constant for loss of $^{\bullet}$OH due to natural sinks (k'_{OH}; blue squares, right y-axis) with PM mass/water mass ratio in three PME3D samples. ($^{\bullet}$OH kinetic measurements were not made in the other two PME3D samples.) Measurements of $^{\bullet}$OH kinetics in the PME3D samples are discussed in Section S1 and shown in Table S3. Using the slopes of the linear relationships to extrapolate P_{OH} and k'_{OH} to values under ambient particle conditions (1 µg-PM/µg-H_2O) gives $P_{OH} = 4.2 \times 10^{-6}$ M s^{-1} and $k'_{OH} = 5.5 \times 10^{9}$ s^{-1}. Error bars represent ± 1 standard error and are too small to be visible for P_{OH}.

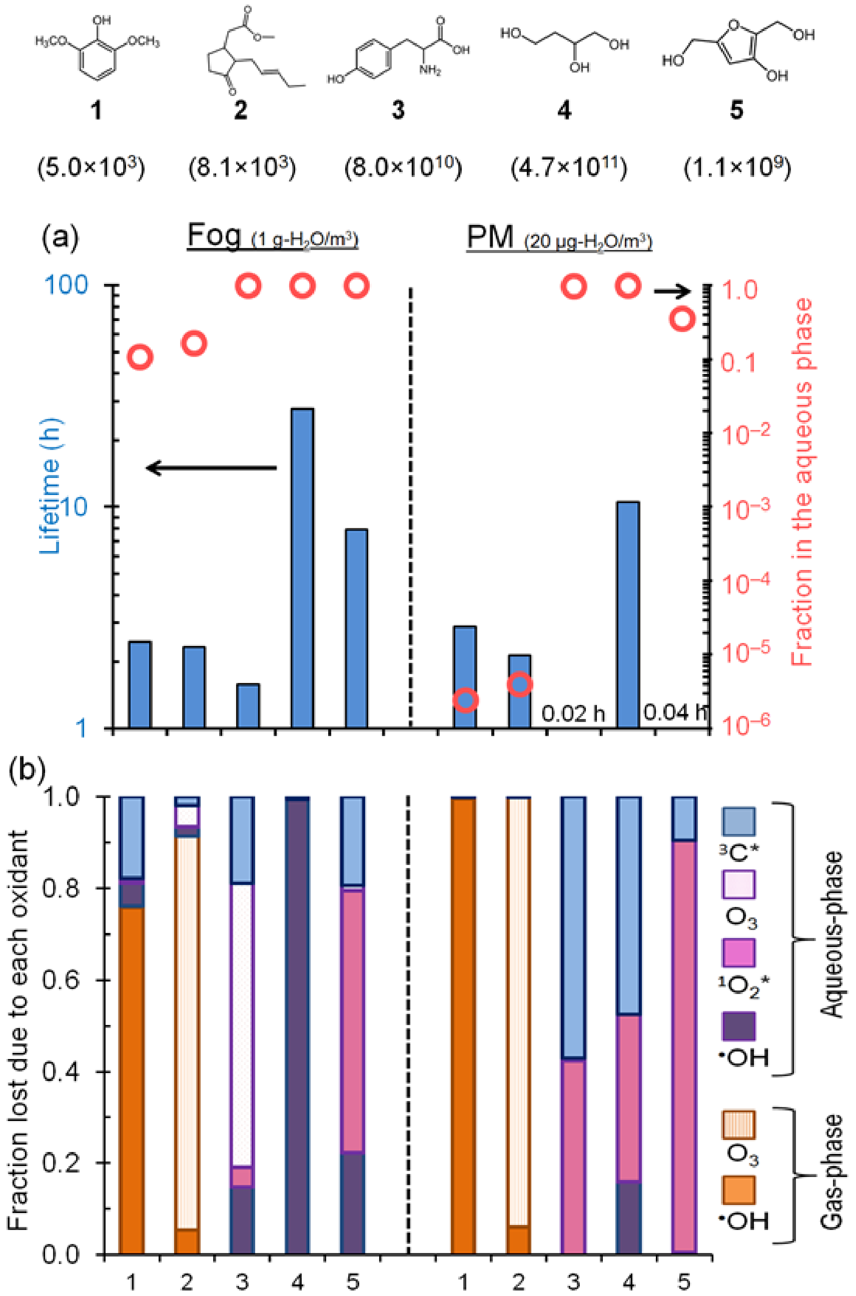

Figure S11. Fate of five model organic compounds – syringol, methyl jasmonate, tyrosine, 1,2,4-butanetriol and 3-hydroxy-2,5-bis(hydroxymethyl)furan – under fog (left of vertical dashed line) and PM (right of dashed line) conditions using an upper-bound estimate for triplet concentrations in PM. Estimated Henry's law constants for the compounds (in units of M atm^{-1}) are in parentheses beneath each structure. Panel (a): the blue columns represent overall lifetimes of the organics via both gas and aqueous-phase loss processes, and the red open circles represent the fractions present in fog or aqueous PM. (b) Fraction of each compound lost via each pathway. The aqueous triplet concentration in PM is 1.5 × 10^{-10} M (Table S15, Fig. 5, main text). All oxidant concentrations and rate constant data are shown in Tables S16 and S17.

S1. Hydroxyl radical measurements in PME3 and PME3D extracts

S1.1: Determining $^{\bullet}$OH steady-state concentrations ([$^{\bullet}$OH])

Typically, for $^{\bullet}$OH measurements we used benzene as the probe. Since benzene is volatile, we performed the illumination in 5 mL sealed quartz cuvettes (instead of quartz tubes) fully filled with extract, only withdrawing 100 µL for analysis at each time point to minimize loss of benzene due to volatilization into the headspace. However, for the PME3D extracts, where we had limited sample volume, we could not fully fill the 5 mL cuvettes. Due to this limitation, for the PME3D samples we monitored the loss of 2-methyl-3-buten-2-ol (MBO) to determine $^{\bullet}$OH concentrations, then separately measured the production rate of $^{\bullet}$OH using benzene (for the three dilutions with sufficient volume), and combined these two measures to determine the $^{\bullet}$OH sink.

There are three main reasons we chose MBO as a probe: 1) it is less volatile than benzene in water, 2) its rate constants with the major photooxidants (i.e. $^{\bullet}$OH, $^1O_2$* and ^3C*) are known, and 3) its reaction with $^{\bullet}$OH is much faster than with $^1O_2$* and ^3C* (see below). Fresh MBO stock was made one day prior to each experiment. 1.0 mL of acidified (pH 4.2) PME3D extract was spiked to 75 µM MBO, capped and illuminated with simulated sunlight in a quartz tube of 4 mm pathlength. Unfortunately, we later realized that this relatively high concentration of MBO was sometimes a significant sink for $^{\bullet}$OH in our PME3 extracts, thus suppressing the apparent steady-state concentration of hydroxyl radical. We are able to approximately correct for this error using an MBO Correction Factor, which is described below.

Throughout the illumination period, MBO loss was measured with HPLC-UV (eluent of 20% acetonitrile: 80% Milli-Q water, flow rate of 0.6 mL/min, detection wavelength of 200 nm and column temperature of 35°C). The pseudo-first-order rate constant for loss of MBO (k'_{MBO}; s^{-1}) was obtained as the negative of the slope of the plot of ln([MBO]/[MBO]$_0$) versus time, then normalized to Davis-winter-solstice light using an analog of Eq. (4) in the main text. Because MBO is not a specific probe for $^{\bullet}$OH, its loss in each sample is the sum of all its loss pathways:

$$k'_{\mathrm{MBO}} = k_{\mathrm{MBO+OH}}\,[^{\bullet}\mathrm{OH}] + k_{\mathrm{MBO+1O2*}}[^1\mathrm{O}_2*] + \Sigma(k_{\mathrm{MBO+3C_i*}}[^3\mathrm{C_i}*]) + j_{\mathrm{MBO}} \qquad \text{(S1)}$$

where [$^{\bullet}$OH], [$^1O_2$*] and $\sum$[^3C_i*] are the steady-state concentrations of the photooxidants. The variables $k_{\mathrm{MBO+OH}}$ (7.4 (± 0.5) × 10^9 M^{-1} s^{-1}; (Richards-Henderson et al., 2014b)), $k_{\mathrm{MBO+1O2*}}$ (7.0 (± 1.0) × 10^5 M^{-1} s^{-1}; (Richards-Henderson et al., 2014b)) and $k_{\mathrm{MBO+3Ci*}}$ (discussed below) are the second-order rate constants for reactions of MBO. j_{MBO} is the rate constant for direct photodegradation of the probe and is negligible for our illumination times (2.7×10^{-7} s^{-1}).

Eq. (S1) has two unknown quantities: 1) [$^{\bullet}$OH] and 2) the loss of MBO due to triplets, i.e., $\Sigma(k_{\mathrm{MBO+3Ci*}}[^3\mathrm{C_i}^*])$. To get [$^{\bullet}$OH], we first estimated MBO loss due to triplets ($\Sigma(k_{\mathrm{MBO+3Ci*}}[^3\mathrm{C_i}^*])$) by using two assumptions about the triplets. Our first assumption is that all loss of the triplet probe syringol is due to ^{3}C* and ^{1}O$_2$*, i.e., $^{\bullet}$OH is a negligible oxidant for SYR, based on our measurements in the other samples, PME1-6, where the fraction of SYR lost due to ^{3}C* and ^{1}O$_2$* (combined) is 91 to 98% (Table S8). While we did measure the loss of methyl jasmonate in the PME3D samples, we only used syringol loss to determine $^{\bullet}$OH concentrations since our first assumption listed above is not valid for MeJA, i.e., we cannot assume that all loss of MeJA is due to ^{3}C* and ^{1}O$_2$* since $^{\bullet}$OH is a significant sink for MeJA (Table S9).

The loss of syringol in the PME3D extracts is the sum of its loss due to $^{\bullet}$OH, ^{1}O$_2$* and ^{3}C*:

$$k'_{\mathrm{SYR}} = k_{\mathrm{SYR+OH}}\,[^{\bullet}\mathrm{OH}] + k_{\mathrm{SYR+1O2*}}[^1\mathrm{O_2}^*] + \Sigma(k_{\mathrm{SYR+3C_i*}}[^3\mathrm{C_i}^*]) \qquad \text{(S2)}$$

Direct photodegradation of syringol is negligible, and the contributions of other oxidants have been previously determined to be small (Section 2.5.3, main text). Based on our first assumption, $k_{\mathrm{SYR+OH}}$ [$^{\bullet}$OH] is much smaller than the sum of the other two terms on the right-hand side of Eq. (S2) and this equation can be simplified to:

$$k'_{\mathrm{SYR}} \approx k_{\mathrm{SYR+1O2*}}[^1\mathrm{O_2}^*] + \Sigma(k_{\mathrm{SYR+3C_i*}}[^3\mathrm{C_i}^*]) \qquad \text{(S3)}$$

Our second assumption is that the reactivity of the triplet mixture in the PM extracts most closely resembles a binary mixture of the model triplets ^{3}3MAP* and ^{3}DMB*– since these are the best triplet matches obtained for majority of the particle extracts (Table S11). For simplicity, we use a 1:1 mixture of the two model triplets. Thus, for $k_{\mathrm{SYR+3Ci*}}$ we used a triplet-syringol rate constant (± σ) of 3.7 (± 0.2) × 10^9 M^{-1} s^{-1}, which is the average of $k_{\mathrm{SYR+3MAP*}}$ and $k_{\mathrm{SYR+3DMB*}}$ (Table S10) in Eq. (S3) to obtain the triplet steady-state concentration:

$$\Sigma[^{3}\mathrm{C_i}^*] = \frac{k'_{\mathrm{SYR}} - (k_{\mathrm{SYR+1O2^*}}[^{1}\mathrm{O_2}^*])}{k_{\mathrm{SYR+3C_i^*}}} \qquad \text{(S4)}$$

Using the measured singlet oxygen concentration, $[^{1}\mathrm{O_2}^*]$, for each PME3 dilution we determine $\Sigma[^{3}\mathrm{C_i}^*]$ in Eq. (S4), which we then plug into Eq. (S1), along with $k_{\mathrm{MBO+3Ci^*}} = 3.4\ (\pm\ 0.4) \times 10^{7}\ \mathrm{M^{-1}\ s^{-1}}$, the average of $k_{\mathrm{MBO+33MAP^*}}$ and $k_{\mathrm{MBO+3DMB^*}}$ (Richards-Henderson et al. (2014b)), to obtain the first iteration of $[^{\bullet}\mathrm{OH}]$:

$$[^{\bullet}\mathrm{OH}] = \frac{k'_{\mathrm{MBO}} - k_{\mathrm{MBO+1O2^*}}[^{1}\mathrm{O_2}^*] - \Sigma(k_{\mathrm{MBO+3C_i^*}}[^{3}\mathrm{Ci}^*])}{k_{\mathrm{MBO+3C_i^*}}} \qquad \text{(S5)}$$

We then remove the first assumption and plug these $[^{\bullet}\mathrm{OH}]$ values into Eq. (S2) to get a second set of $\Sigma[^{3}\mathrm{C_i}^*]$ values, which we use in Eq. (S1) to obtain the second iteration of $[^{\bullet}\mathrm{OH}]$. We continue this iterative process until the $[^{\bullet}\mathrm{OH}]$ values change by less than 0.01% (Table S18).

Table S18. Determination of hydroxyl radical steady-state concentrations, $[^{\bullet}\mathrm{OH}]$, from results of the MBO experiments

	[OH] from Iterations, 10^{-16} M						
Sample ID	Iteration 1	Iteration 2	Iteration 3	Iteration 4	MBO Correction Factor	$1/S_{\lambda}$	Final $[^{\bullet}\mathrm{OH}]$ 10^{-16} M
PME3D0.5	5.54 (1.87)	5.72 (1.93)	5.73 (1.93)	5.73 (1.39)	1.10	1.15	7.3 (1.8)
PME3D1	5.74 (1.91)	5.93 (1.97)	5.94 (1.97)	5.94 (1.40)	1.24	1.07	7.9 (1.9)
PME3D1.3	2.23 (0.76)	2.31 (0.77)	2.31 (0.79)	2.31 (0.57)	1.27	1.05	3.0 (0.8)
PME3D2.5*	2.19 (0.75)	2.26 (0.77)	2.26 (0.77)	2.26 (0.57)	1.43	1.03	3.3 (1.0)
PME3D10	1.89 (0.68)	1.95 (0.70)	1.95 (0.70)	1.95 (0.54)	3.31	1.01	6.6 (2.8)

Uncertainties in parentheses are ± 1 standard error.

We then made two corrections to the fourth (and final) iteration values. The first, and largest, correction was to account for the scavenging of $^{\bullet}$OH by MBO by multiplying by an “MBO Correction Factor”. This correction factor is the sum of the pseudo-first-order rate constants for MBO and natural scavengers divided by the pseudo-first-order rate constant for natural scavengers. As shown in Table S18, this correction increases as the sample gets more dilute: values range from a modest 1.10 in the most concentrated extract to a very large 3.31 in the most dilute extract. The second correction was to divide by the light screening factor, S_{λ} (Table S1 and Sect. 2.5.1 of main text) to account for light absorption in our container; since the light screening factors are close to 1 (i.e., 0.87 – 0.99), these corrections are relatively small. The standard errors on the final $^{\bullet}$OH concentrations account for both the experimental uncertainty as well as the uncertainty associated with the MBO correction factor.

S1.2: Rate of $^{\bullet}$OH photoproduction (P_{OH})

Similar to the other extracts, in the PME3 samples we used benzene as the probe measure $^{\bullet}$OH photoformation (Kaur and Anastasio, 2017; Anastasio and McGregor, 2001; Zhou and Mopper, 1990). A 5.0 mL aliquot of extract was acidified to pH 4.2 (± 0.2) and spiked with 1500 μM benzene, which should scavenge essentially all $^{\bullet}$OH. The solution was illuminated in a capped, sealed quartz cuvette with a 1 cm pathlength (Sect. 2.5.1 in main text). In all cases, phenol concentration increased linearly with time, and the rate of phenol formation (R_P) was obtained as the slope of the plot of phenol concentration versus time. We then plotted $1/R_p$ versus 1/[Benzene] and the intercept of that plot gave the experimentally measured rate of $^{\bullet}$OH photoproduction ($P_{OH,EXP}$) (Zhou and Mopper, 1990). Measured rates of $^{\bullet}$OH formation were normalized to the rate expected under midday Davis, CA winter-solstice sunlight (P_{OH}) based on 2-nitrobenzaldehyde (2NB) actinometry:

$$P_{OH} = P_{OH,EXP} \times \frac{j_{2NB,WIN}}{j_{2NB,EXP}} \qquad (S6)$$

where $j_{2NB,WIN}$ is the rate constant for loss of 2NB measured at midday near the winter solstice in Davis (0.0070 s^{-1}; Anastasio and McGregor, (2001)), and $j_{2NB,EXP}$ is the measured rate constant for loss of 2NB on the day of the experiment. Due to the volume requirements of this technique, we were only able to measure P_{OH} in three extracts – PME3, PME3D2.5* and PME3D10.

S1.3 Rate constant for loss of $^{\bullet}$OH due to natural sinks (k'_{OH})

In the PME3 samples we calculated the pseudo-first-order rate constant for loss of $^{\bullet}$OH due to natural sinks by dividing the measured rate of $^{\bullet}$OH photoproduction determined with benzene (Sect. S1.2) by the measured $^{\bullet}$OH steady-state concentration determined with MBO (Sect. S1.1):

$$k'_{OH} = \frac{P_{OH}}{[\bullet OH]} \quad (S7)$$

S2. $^{\bullet}$OH sink measurements (k'_{OH}) in field blanks FB1 and FB2

We also measured the rate constant for loss of $^{\bullet}$OH due to natural sinks (k'_{OH}) in field blank FB1, which was extracted under the "dilute conditions", i.e. each 2 × 2 cm filter square was extracted in 2.5 mL Milli-Q.

In the early stages of this project, we used benzoate as an $^{\bullet}$OH probe (Anastasio and McGregor, 2001), which reacts with $^{\bullet}$OH to form m-hydroxybenzoic acid, m-HBA (and other products), which was quantified using UV-HPLC. Four 5.0 mL aliquots of extract were spiked with 100–1500 µM of sodium benzoate/benzoic acid solution (20 mM) at pH 4.2. Since P_{OH} in FB1 was below our detection limit (Table S3), we added 200 µM hydrogen peroxide as an $^{\bullet}$OH source to each aliquot in order to measure the $^{\bullet}$OH sinks. Aliquots were illuminated in capped quartz tubes with a 0.4 cm pathlength (Sect. 2.3 main text). The formation of m-HBA was linear in all cases, and the slope of the plot of [m-HBA] versus time in each aliquot is the rate of m-HBA formation (R_P, µM min^{-1}). Similar to the benzene technique, we then plotted 1/R_P versus 1/[benzoate], used the slope and y-intercept of the inverse plot to obtain P_{OH}, k'_{OH} and [$^{\bullet}$OH], which were normalized to Davis midday solstice sunlight conditions. k'_{OH} measured using benzoate was 4.4 (± 0.5) × 10^5 s^{-1}, and represented 56% of the dilute sample average (PME1*, PME2*, PME3D2.5). Because this is high, we ran a number of tests to identify the source of the background $^{\bullet}$OH sinks in FB1, starting with measuring k'_{OH} in two Milli-Q solutions containing only HOOH and probe stocks to identify whether these were the source of contamination. k'_{OH} in Milli-Q was nearly as high as in FB1: even after rigorously cleaning the quartz tubes using a UV+HOOH treatment (Chen et al., 2016), k'_{OH} was not lowered appreciably (Fig. S12). Since at this point, it appeared that the probe chemicals (sodium benzoate and benzoic acid) could be contaminated, we decided to switch to benzene as the $^{\bullet}$OH probe.

The experimental procedure for the benzene technique is very similar to the benzoate technique, except that the aliquots of FB1 were acidified to pH 4.2 (± 0.2) using 10 mM sulfuric acid. While the k'_{OH} value using benzene was slightly lower than the benzoate case (3.4 (± 0.4) × 10^5 s^{-1}), it still represented 43% of the PM sample average. We then performed the benzene technique in Milli-Q water: the resulting k'_{OH} of 1.2 (± 0.1) × 10^4 s^{-1} was more than 10 times lower than the other measurements, typical of solutions without any background organic contamination (Chen et al., 2016). This was the lowest k'_{OH} measured in our trials so, we chose to proceed with benzene as the probe for measuring $^{\bullet}OH$ in the particle extracts.

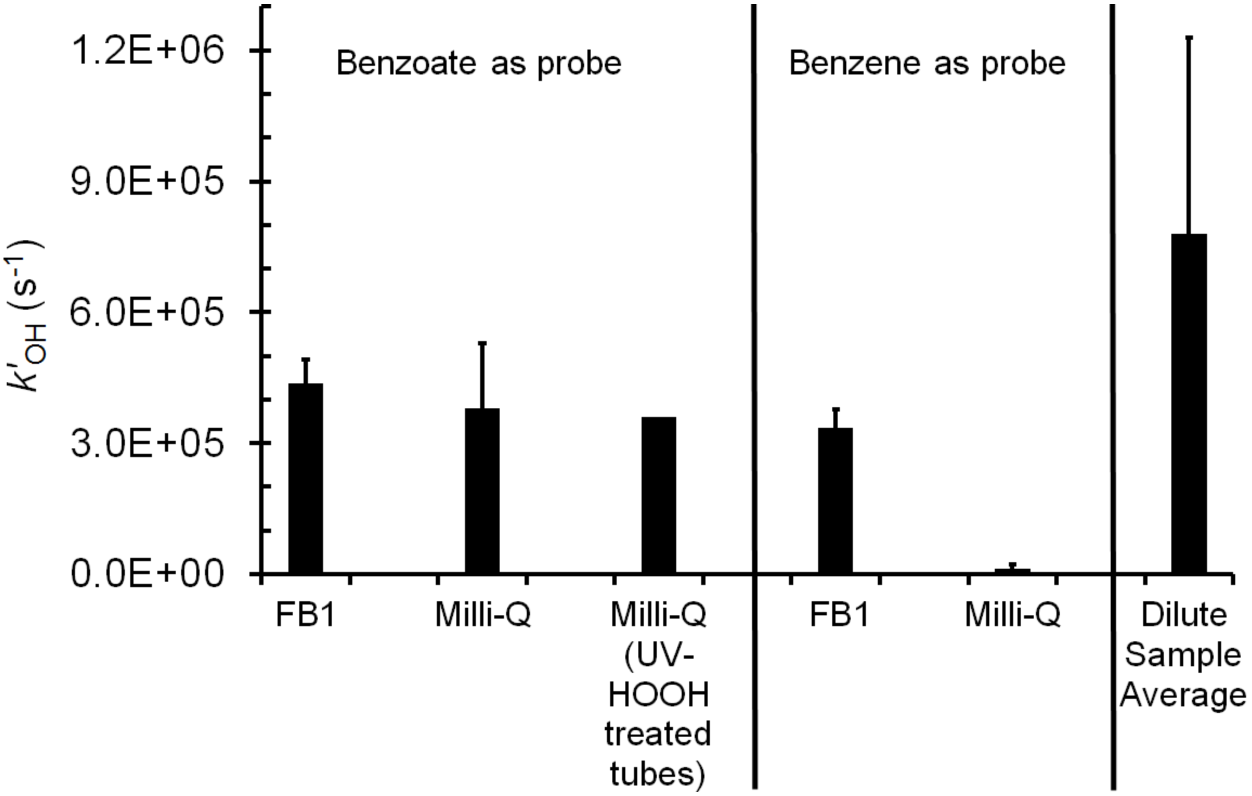

Figure S12. Measured pseudo-first-order rate constant for loss of $^{\bullet}OH$ due to natural sinks (k'_{OH}) in various solutions using sodium benzoate/benzoic acid and benzene as $^{\bullet}OH$ probes. Samples labeled "Milli-Q" contain only probe and HOOH. Samples labeled "FB1" are measurements in the extract solution of Field Blank 1. "Dilute Sample Average" is the average of the k'_{OH} measurements in PME1*, PME2* and PME3D2.5* (Table S3).

We next determined k'_{OH} in FB2 with benzene under standard extract conditions (1 mL Milli-Q per filter square). However, the resulting value of 2.7 (± 0.1) × 10^5 s^{-1} is not much lower than the value in (more dilute) FB1 determined with benzoate and is 20 times higher than the Milli-Q value. But because the k'_{OH} value in the standard extracts (PME3D1-PME6) is high (Table S3), the corresponding FB2 value is only 11% of the standard sample average. One plausible contributing factor to the high k'_{OH} in the field blanks is that organic matter is coming off the filter material during extraction; we see this in the DOC measurements for both field blanks (Table S2). For future studies, we recommend first evaluating a few different types of particle filters by making background k'_{OH} measurements and then picking the filters that introduce the least contamination.

We did not adjust values of k'_{OH} measured in the particle extracts for the field blank rate constants. If we had adjusted them, $^{\bullet}$OH concentrations would have increased by 50% in the "dilute" extracts and by 10% in the standard extracts. However, the concentrations would still be similar to fog. Additionally, this adjustment would have no effect on the extrapolation to ambient PM conditions, since [$^{\bullet}$OH] in all PME3D extracts would go up equally.

S3. Other oxidants in PM extracts

Since the probes we use for triplet determination do not react with only triplets (Eq. (5), main text), we account for the contributions of $^1O_2^*$ and $^\bullet OH$ to probe loss. However, it is also possible that other oxidants (that we do not measure) are also contributing to triplet probe loss. Here we examine this possibility for triplet probe loss in the PM extracts. In our previous measurements of photooxidants in fog water (Kaur and Anastasio, 2018), we estimated the importance of hydroperoxyl radical/superoxide radical anion ($HO_2^\bullet/^\bullet O_2^-$), ozone ($O_3$), carbonate radical ($^\bullet CO_3^-$) and hydrogen ion/hydrated electron ($H^\bullet$ (aq)/e^-(aq)) and found that these species in total contributed less than 7 % to the average measured syringol loss. To do this calculation for our PM extracts, we estimate the steady-state concentrations of these oxidants in the illuminated extracts and, using reaction rate constants available in literature, calculate a pseudo-first-order rate constant for their reaction with syringol. We then compare that to the average (± σ) measured syringol loss in the standard extracts, $k'_{SYR} = 3.9\ (\pm\ 1.3) \times 10^{-4}\ s^{-1}$. As we noted in our previous paper, there are insufficient rate constants in the literature for reactions of methyl jasmonate in order to estimate its potential loss to other oxidants.

Hydroperoxyl Radical / Superoxide Radical Anion (O_2 (-I))

Hydroperoxyl radical and superoxide radical anion (i.e., O_2(-I)) are a conjugate acid-base pair; the pK_a of $HO_2^\bullet$ is 4.75 ± 0.08 (Bielski et al., 1985). Since the pH of our extracts was adjusted to ambient particle pH of 4.2 (Parworth et al., 2017), the mole fractions of $HO_2^\bullet$ and $^\bullet O_2^-$ in the extracts are 0.78 and 0.22, respectively. There are no rate constants available for reaction of either species with syringol (2,6-dimethoxyphenol) so we use the fastest reported rate constants for reactions of similar compounds with $^\bullet O_2^-$ and $HO_2^\bullet$. For substituted phenols, the rate constant for reaction of $^\bullet O_2^-$ with guaiacol (2-methoxyphenol) is $2.5 \times 10^3\ M^{-1}s^{-1}$ (Yasuhisa et al., 1993); for $HO_2^\bullet$, the rate constant with catechol (1,2-benzenediol) is $4.7 \times 10^4\ M^{-1}\ s^{-1}$ (Bielski, 1983). At pH 4.2, the mole-fraction weighted rate constant, used as the proxy for $k_{SYR+O2(-I)}$, is $3.7 \times 10^4\ M^{-1}s^{-1}$.

To estimate O_2(-I) concentrations in the extracts, we use previously measured rates of HOOH formation in illuminated fog waters from California's Central Valley since these two oxidants are intimately connected (Deguillaume et al., 2004; Anastasio, 1994):

$O_2(\text{-I}) + \text{Cu(I)} \rightarrow \text{HOOH} + \text{Cu(II)}$ (S8)

The maximum measured production rate of HOOH, P_{HOOH} , in illuminated Central Valley fogs is 3 µM h^{-1} (8.3×10^{-10} M s^{-1}; Anastasio (1994)) . We expect that P_{HOOH} in particle extracts will be higher than fog, so we use an enhancement factor based on the observed increase in singlet oxygen concentrations in the standard extracts, which is a factor of seven higher than Davis fog average (Table S7). The reaction rate constants for $^{\bullet}O_2^{-}$ and $HO_2^{\bullet}$ reacting with Cu(I) are 9.4×10^9 M^{-1} s^{-1} (Piechowski et al., 1993) and 3.5×10^9 M^{-1} s^{-1} (Berdnikov, 1973), respectively, which gives an overall, mole-fraction-weighted reaction rate constant, $k_{\text{O2(-I)+Cu(I)}}$, of 4.8×10^9 M^{-1} s^{-1}. We assume that the Cu(I) concentration is similar to that of O_2(-I) (e.g., [Cu(I)] ≈ 1 nM in the daytime urban cloud scenario of Deguillaume et al. (2004)). Solving the rate equation for S8 with these inputs gives an O_2(-I) steady-state concentration of 1.1×10^{-9} M. At this concentration, the estimated loss rate constant for syringol due to O_2(-I), $k'_{\text{SYR,O2(-I)}}$ is 4.1×10^{-5} s^{-1}, which would account for 11 % of the average observed syringol loss. This suggests that superoxide is a minor sink for syringol in our samples, although it does appear to be more significant in particle extracts than fog.

Ozone (O_3)

Based on the Henry's law constant for ozone at 25°C ($K_H = 1.1 \times 10^{-2}$ M atm^{-1} (Seinfeld and Pandis, 2012) and assuming a gas-phase mixing ratio for O_3 of 30 ppbv, gives an initial aqueous-phase concentration of ozone in our samples of 3.3×10^{-10} M. The actual concentration is likely lower since our samples are capped during illumination. The bimolecular rate constant for reaction of ozone with syringol is not available in the literature, so we estimate the rate constant by using the value for phenol ($k_{\text{PhOH+O}_3} = 1.3 \times 10^3$ M^{-1} s^{-1}) (Hoigné and Bader, 1983)with an enhancement factor of 10 based on the measured ratio of phenol and syringol rate constants for reaction with ^{3}DMB* (Smith et al., 2015). Under these assumptions, ozone is a very minor sink for syringol in the fog samples ($k'_{\text{SYR,O}_3} = 4.3 \times 10^{-6}$ s^{-1}), accounting for 1% of the average measured syringol loss.

Carbonate Radical ($^{\bullet}CO_3^{-}$)

The carbonate radical is formed mainly from the reactions of bicarbonate (HCO_3^{-}) and carbonate (CO_3^{2-}) ions with $^{\bullet}$OH and triplet CDOM species. Although DOM components are likely important sinks for $^{\bullet}CO_3^{-}$, this quenching is poorly understood (Canonica et al., 2005; Vione et al., 2014; Huang and Mabury, 2000). There are no published measurements of $^{\bullet}CO_3^{-}$ in atmospheric waters, so we use the typical steady-state concentration measured in surface waters of 2×10^{-14} M determined using N,N-dimethylaniline as a probe (Huang and Mabury, 2000; Zeng and Arnold, 2012). There are concerns that aniline probes overestimate $^{\bullet}CO_3^{-}$ since they also react rapidly with triplets (Rosario-Ortiz and Canonica, 2016), so we treat this as an upper-bound estimate. We do not apply an enhancement factor in this case since DOM appears to play the dual role of source and sink. While $^{\bullet}CO_3^{-}$ reacts rapidly with electron-rich phenolates (i.e., a deprotonated phenol), at pH 4.2 syringol is in the neutral, less reactive form. There are no rate constants available for $^{\bullet}CO_3^{-}$ reacting with methoxyphenols, so we assume the value with SYR is 10 times higher than that with phenol (4.9×10^{6} $M^{-1}s^{-1}$; Chen et al. (1975)). This results in a pseudo-first-order rate constant for loss of SYR due to carbonate radical of 1×10^{-6} s^{-1}, which represents a negligible 0.3% of the average measured syringol loss rate constant in our standard PM extracts.

Hydrogen Ion / Aquated Electron ($H^{\bullet}_{(aq)}/e^{-}_{(aq)}$)

Hydrogen ion ($H^{\bullet}$) and aquated electron ($e^{-}_{(aq)}$) can be formed during irradiation or illumination of dissolved organic matter in natural waters; these exist as a conjugate acid-base pair with a pK_a of 9.6 (Kozmér et al., 2014; Buxton et al., 1988a). In our extracts at pH 4.2, the predominant species would be $H^{\bullet}$ (aq). Zepp et al. (1987) determined an average steady-state concentration of $e^{-}_{(aq)}$ in sunlight-illuminated lake waters to be 1.2×10^{-17} M. Similar to $^{1}O_2$*, since DOM is the main source of $e^{-}_{(aq)}$, we assume an enhancement factor of seven in the steady-state concentration of $e^{-}_{(aq)}$. As an upper bound, we assume the $H^{\bullet}$ concentration to be equal to this. The rate constant for syringol reacting with $H^{\bullet}$ is not known. Using the average rate constant for methoxyphenol, 2.1×10^{9} $M^{-1}s^{-1}$ (O'Neill et al., 1975; Neta and Schuler, 1972), the pseudo-first-order rate constant for loss of SYR due to hydrogen ion is 1.7×10^{-7} s^{-1}, which would account for only 0.04% of the average observed syringol loss.

Combined Contributions from Other Oxidants

Based on our upper-bound estimates, the total rate constant for loss of syringol due to $HO_2^{\bullet}/^{\bullet}O_2^{-}$, O_3, $^{\bullet}CO_3^{-}$ and $H^{\bullet}$ (aq)/e-(aq) is ~ 4.6×10^{-5} s^{-1}, which is only 12% of the average measured syringol loss rate constant. Since this is small, our assumption that the loss of syringol is mainly due to $^{\bullet}$OH, $^1O_2$* and ^{3}C*(Eq. (6), main text) seems valid.

S4. Impacts of mass transport and increasing organic concentration on estimates of aqueous photooxidant concentrations in ambient particles

The steady-state concentration of an oxidant reflects the balance between its rate of formation (P_{OX}) and first-order rate constant for loss ($k'_{OX} = 1 / \tau_{OX}$):

$$[OX] = P_{OX} / k'_{OX} \qquad \text{(S9)}$$

where k'_{OX} is the sum of all the pseudo-first-order sinks of the oxidant. We can use our oxidant measurements for the dilution series of sample PME3 to estimate how the aqueous formation rate and rate constant for loss vary with solute concentration. But extrapolating these results to particle liquid water conditions requires accounting for additional factors, such as mass transport. Here we combine our aqueous measurements with estimates of these other factors to better estimate oxidant concentrations from dilute fog or cloud drop conditions (i.e., a PM solute mass/water mass ratio of 3×10^{-5} μg-PM/μg-H_2O) to a particle liquid water condition (1 μg-PM/μg-H_2O). We roughly estimate the gas-phase influence using a simplified case assuming a temperature of 298 K, total pressure of 1 atm, an aqueous particle radius (R_p) of 0.5 μm at a PM mass/water mass ratio of 1 μg-PM/μg-H_2O, and a constant particle/drop density of 1 g cm^{-3}.

In the case of hydroxyl radical, based on our current measurements and previous work (Arakaki et al., 2013; Anastasio and Newberg, 2007), the concentrations of the major aqueous sources (nitrate, nitrite, and unknown species) and sinks (organic compounds) both scale linearly with PM aqueous mass concentration, indicating that [$^{\bullet}$OH] should be independent of dilution. However, this does not consider the influence of the gas phase. The extremely short lifetime of $^{\bullet}$OH in the particles ($1/k'_{OH} \sim 2 \times 10^{-10}$ s) indicates that this oxidant will not be at Henry's law equilibrium and that the gas phase will be a source of $^{\bullet}$OH. We estimate the rate of this gas-phase mass transport to the particles (P_{MT}) using the Fuchs-Sutugin transition regime formula (Seinfeld and Pandis, 2012) with an estimated gas-phase $^{\bullet}$OH concentration of 1×10^6 molecules cm^{-3} and a mass accommodation coefficient of 1. Under these conditions the drop-volume-normalized rate of $^{\bullet}$OH gas-to-particle transport increases from 7.7×10^{-10} M s^{-1} in dilute drops (3×10^{-5} μg-PM/μg-H_2O) to 4.2×10^{-7} M s^{-1} under particle conditions (1 μg-PM/μg-H_2O). Over this same range, the aqueous photoformation of $^{\bullet}$OH increases even more strongly, from 1.3×10^{-10} M s^{-1} to 4.2×10^{-6} M s^{-1}, respectively. Thus the contribution of gas-phase mass transport to the overall

$^{\bullet}$OH formation rate decreases as the drops become more concentrated, dropping from 86% in the dilute drops to 9% in the particle condition. Considering both the aqueous- and gas-phase sources of $^{\bullet}$OH to the particles, we estimate the steady-state concentration at any dilution using

$$[^{\bullet}\mathrm{OH(aq)}] = (P_{\mathrm{OH}} + P_{\mathrm{MT}})/k'_{\mathrm{OH}} \qquad \text{(S10)}$$

These overall steady-state concentrations range from 5.4×10^{-15} M in the dilute drop condition to 8.4×10^{-16} M in the particle condition, as shown by the solid orange line in Figure 5.

In the case of singlet molecular oxygen, there is little gas-phase data, but past estimates suggested concentrations on the order of 1×10^{8} molecules cm^{-3} (Demerjian, 1974). At Henry's law equilibrium, this gas-phase concentration corresponds to an aqueous concentration of 5×10^{-14} M (using the Henry's law constant for ground state O_2, 1.3×10^{-3} M atm^{-1} at 298 K; Seinfeld and Pandis (2012)). This estimated aqueous concentration is somewhat smaller than our measured concentrations in dilute extracts (Table S7), which are approximately as concentrated as fog/cloud drops, and many orders of magnitude lower than our extrapolated particle concentrations. Thus the net effect of mass transport will be to move $^{1}O_2^{*}$ from the particles to the gas phase. As an upper bound, the fastest step in evaporation of $^{1}O_2^{*}$ is likely liquid-phase diffusion, which has a characteristic time (Seinfeld and Pandis, 2012) of

$$\tau_{\mathrm{LD}} = R_p^{2}/(\pi^{2}\times D_{\mathrm{aq}}) \qquad \text{(S11)}$$

where D_{aq} is the aqueous diffusion coefficient, approximately 1×10^{-5} cm^{2} s^{-1} if we assume an aqueous particle. Calculated liquid-phase diffusion lifetimes range from 3×10^{-5} s for particles (1 µg-PM/µg-H_2O and an assumed radius of 0.5 µm) to 0.02 s for dilute drops (3×10^{-5} µg-PM/µg-H_2O, which corresponds to a radius of 13 µm). The inverse of τ_{LD} is the approximate first-order rate constant for liquid-phase diffusion, k'_{LD}; values range from 60 s in dilute drops to 4×10^{4} s^{-1} in particles. These values are low compared to the first-order rate constant for deactivation of $^{1}O_2^{*}$ in water ($k'_{\mathrm{H2O}} = 2.2 \times 10^{5}$ s^{-1}; Bilski et al. (1997)), indicating that evaporation is a minor sink.

Under cloud and fog drop conditions (and in our PM extracts) deactivation by water is the major sink for singlet oxygen, but under the more concentrated conditions of aqueous particles, organic compounds might also be important. To very roughly estimate this organic sink, we multiply our average DOC concentration in PM extracts (3.4 mM-C; Table S2) by a factor of 1000 to extrapolate to ambient PM conditions and assume all of this material is soluble, resulting in an aqueous concentration of particulate organics of 3.4 M-C. If each organic molecule has an average of 6 C atoms (i.e., the average is the same as levoglucosan), this corresponds to a water-soluble organic molecule concentration of 0.56 mol-compounds L^{-1}. We apportion this total concentration based on the emissions measurements of Jen et al. (2019), where water-soluble organics in biomass burning emissions are roughly 50% sugars, 25% phenols, and 25% organic nitrogen. Table S19 below shows the resulting estimated particle concentrations, along with an estimated average rate constant for each class based on the compilation by Wilkinson et al. (1995). Summing the contributions from each compound class we estimate a total pseudo-first order rate constant for loss of $^1O_2*$ by soluble organics in the particles (at 1 μg-PM/μg-H_2O) of 2.8×10^6 s^{-1}. We linearly scale this sink, k'_{ORG}, by the PM mass/water mass ratio of the drops and particles to address dilution effects; e.g., for particles with 0.1 μg-PM/μg-H_2O, $k'_{ORG} = 2.8 \times 10^5$ s^{-1}.

Table S 19. Estimates of the organic sink of $^1O_2*$ in aqueous particles at 1 μg-PM/μg-H_2O

Compound Class	Dissolved Concentration (M)	2^{nd}-order Rate Constant Range (M^{-1} s^{-1})	Assumed 2^{nd}-order k (M^{-1} s^{-1})	k'_{ORG} (s^{-1})
Sugars	0.28	10^4	10^4	2800
Phenols	0.14	10^6 - 10^7	10^7	1.4×10^6
Organic Nitrogen	0.14	10^3 – 10^9	10^7	1.4×10^6

The resulting estimate for the steady-state concentration of $^1O_2*$ in drops and particles is

$$[^1O_2*] = P_{1O2*} / (k'_{H2O} + k'_{LD} + k'_{ORG}) \qquad \text{(S12)}$$

where the numerator, i.e., the rate of $^1O_2*$ photoformation increases with increasing solute concentration according to the linear regression of our PME3D values (with the y-intercept fixed at zero): $P_{1O2*} = 5.0 \times 10^{-4}$ M s^{-1}/(μg-PM/μg-water). This gives rates of singlet oxygen formation that range from 1.5×10^{-8} M s^{-1} in dilute drops to 5.0×10^{-4} M s^{-1} for our standard particle condition. The denominator of Eq. S12 is 2.2×10^{5} s^{-1} in dilute drops and remains at this value until the particle concentration reaches 10^{-3} μg-PM/μg-water, at which point it increases because of the increasingly concentrated organic sinks. At the particle condition of 1 μg-PM/μg-H_2O, the denominator is 3.1×10^{6} s^{-1} and organic sinks account for 92% of $^1O_2*$ loss. Calculated values of [$^1O_2*$] range from 6.7×10^{-14} M in dilute drops to 1.6×10^{-10} M for the particle liquid water condition.

For triplet excited states we fit our experimental data to a hyperbolic fit:

$$[^3C^*] = \frac{a\,[m_{PM}/m_{H2O}]}{1+b\,[m_{PM}/m_{H2O}]} \qquad \text{(S13)}$$

where m_{PM}/m_{H2O} is the PM mass/water mass ratio, the numerator represents the formation of triplets and the denominator represents the sinks. We fit our experimental data to this equation in Excel in two ways: (1) a best fit, where the hyperbolic equation parameters were tuned to minimize the regression error, and (2) a high estimate fit, where the parameters were tuned so that the regression line passed near the top of the error bar for the most concentrated sample extract (PME3D0.5). The parameters for these two fits are: (1) $a = 3.08 \times 10^{-10}$ M and $b = 1.31 \times 10^{3}$, and (2) $a = 2.26 \times 10^{-10}$ M and $b = 17.0$. We did not include the data point for PME3D10 when determining the regression fits (but do show it in the plots) because of the larger uncertainty in its triplet concentration, a result of the significant $^\bullet$OH perturbation by MBO in this most dilute sample. Our interpretation of the curvature in these regression fits (Figure 5) is that as the solutions get more concentrated, organics become the major triplet sink, causing [$^3C^*$] to plateau at higher PM mass/water mass ratios; we estimate the size of this organic sink in the next section. Thus, these fits should account for the organic sinks that will be important under particle conditions.

To a first approximation, we expect that mass transport will have no significant impact on the concentrations of triplets. Since most of the BrC precursors for $^3C^*$ are likely in the particle phase (rather than the gas phase) we expect that gas-phase concentrations of triplets are relatively small and that the gas phase is not a significant source of triplets to the particles. We also expect that evaporation of triplets is minor since their lifetimes are relatively short (1 μs based just on

O_2 as a sink) and their gas-particle partitioning (like that of their BrC precursors) is strongly tilted toward the particle phase. Thus we assume that the particle concentration of triplets is relatively unaffected by mass transport.

S5. Estimating triplet characteristics in particle extract PME3

We can use our measurements of triplet steady-state concentrations in the PME3 dilution series to derive the first-order rate constant for triplet formation and the overall rate constant for triplet reaction and quenching by DOC. The rate of triplet formation (P_{3C*}) from the photoexcitation of chromophores 'C' in the extracts can be expressed as:

$$P_{3C*} = j_{abs} \times \Phi_{ISC} \times [C] \qquad \text{(S14)}$$

where j_{abs} is the rate constant for light absorption (s^{-1}) by C and Φ_{ISC} is the intersystem crossing quantum yield, i.e., the fraction of the first excited single state, S_1, that forms the lowest triplet excited state, T_1. Assuming the chromophore concentration is a fraction f (mole-chromophore mole-C^{-1}) of the DOC concentration (mole-C L^{-1}), the rate of triplet formation can be expressed as

$$P_{3C*} = j_{abs} \times \Phi_{ISC} \times f \times [DOC] \qquad \text{(S15)}$$

The rate constant for loss of the triplet (k'_{3C*}; s^{-1}) in an extract is the sum of all its loss pathways:

$$k'_{3C*} = k_{3C*+O2}\,[O_2] + k_{rxn}\,[DOC] + k_Q\,[DOC] \qquad \text{(S16)}$$

where k_{3C*+O2} is the bimolecular rate constant for O_2 quenching (we use the average value for the three model triplets with measurements, 2.8 (± 0.4) × 10^9 $M^{-1}s^{-1}$; Table S11); $[O_2]$ is the dissolved oxygen concentration (284 μM at 20 °C) (USGS, 2018); k_{rxn} ($M^{-1}s^{-1}$) is the rate constant for reaction of triplet with dissolved organics; and k_Q ($M^{-1}s^{-1}$) is the rate constant for the non-reactive quenching of triplet by DOC (Smith et al., 2014).

Assuming steady state, the triplet concentration is the ratio of its rate of photoproduction and its rate constant for loss:

$$[^3\mathrm{C}^*] = \frac{P3C*}{k'3C*} = \frac{jabs \times \Phi ISC \times f \times [DOC]}{k3C{*}{+}O2\ [O2] + (krxn + kQ)\ [DOC]} \qquad \text{(S17)}$$

This can be re-written as

$$[^3\mathrm{C}^*] = \frac{\left(\frac{jabs \times \Phi ISC \times f}{k3C{*}{+}O2\ [O2]}\right) \times [DOC]}{1 + \left(\frac{krxn + kQ}{k3C{*}{+}O2\ [O2]}\right) \times [DOC]} \qquad \text{(S18)}$$

We then fit our triplet steady-state concentration measurements in the PME3D extracts to the following two-parameter equation:

$$[^3\mathrm{C}^*] = \frac{c\ [DOC]}{1 + d\ [DOC]} \qquad \text{(S19)}$$

The regression fit is shown in Fig. S13; the parameters for the fit obtained using Excel are c = 2.9×10^{-11} and d = 117 M^{-1}; we did not include the data point for PME3D10 in determining the regression fit because of the larger uncertainty in its triplet concentration, a result of the significant probe perturbation in this most dilute sample. Using the regression parameters, we calculate that the rate constant for triplet formation, i.e., $j_{abs} \times \Phi_{\mathrm{ISC}} \times f$, is 2.3 (± 0.3) × 10^{-5} s^{-1} and the sum of the reaction and quenching rate constants for the triplets by DOC, i.e.,$k_{\mathrm{rxn}} + k_{\mathrm{Q}}$, is 9.3 (± 1.3) × 10^{7} L mol-C^{-1} s^{-1}.

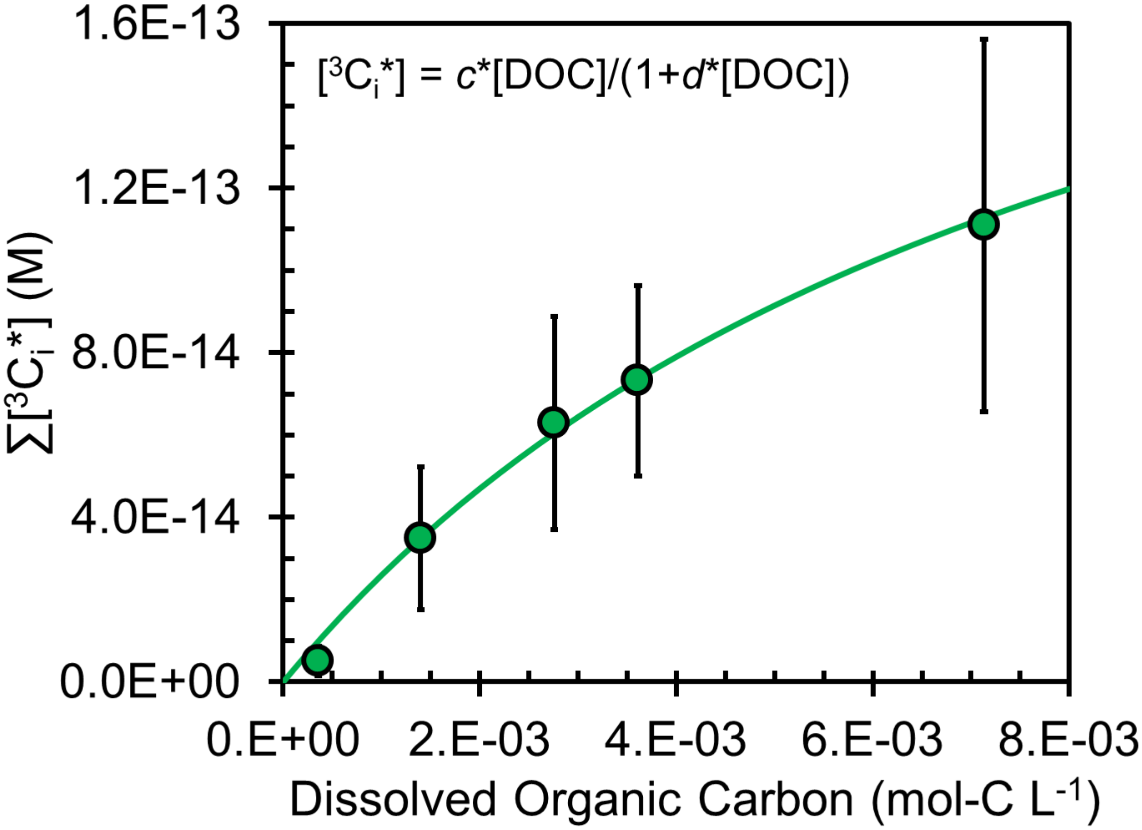

Figure S13. Change in triplet steady-state concentration with dissolved organic carbon concentration in the PME3D extracts. Error bars represent ± 1 standard error in measured triplet concentrations (Table S13). The regression line is a fit of Equation S19 to the experimental data in Excel, yielding parameter estimates of $c = 2.90 \times 10^{-11}$ and $d = 117\ \mathrm{M}^{-1}$. The PME3D10 point was not included in the regression fit (although is shown on the plot) because of issues with too-high probe concentrations in the $^{\bullet}$OH determination. The DOC value for sample PME3D0.5 (which had very limited volume) is estimated based on results for the other four dilutions and given in Table S2.

S6. References

Anastasio, C.: Aqueous phase photochemical formation of hydrogen peroxide in authentic atmospheric waters and model compound solutions, Ph.D. Dissertation, Duke University, 1994.

Anastasio, C., and McGregor, K. G.: Chemistry of fog waters in California's central valley: 1. In situ photoformation of hydroxyl radical and singlet molecular oxygen, Atmospheric Environment, 35, 1079-1089, 2001.

Anastasio, C., and Newberg, J. T.: Sources and sinks of hydroxyl radical in sea-salt particles, J. Geophys. Res., 112, D10306, 2007.

Anbar, M., Meyerstein, D., and Neta, P.: Reactivity of aliphatic compounds towards hydroxyl radicals, Journal of the Chemical Society B: Physical Organic, 742-747, 1966.

Andreev, P. Y.: Reaction of ozone with five-membered hetarenes in a liquid phase, Russ. J. Appl. Chem., 85, 1395-1398, 2012.

Arakaki, T., Anastasio, C., Kuroki, Y., Nakajima, H., Okada, K., Kotani, Y., Handa, D., Azechi, S., Kimura, T., Tsuhako, A., and Miyagi, Y.: A general scavenging rate constant for reaction of hydroxyl radical with organic carbon in atmospheric waters, Environ. Sci. Technol., 47, 8196-8203, 2013.

Atkinson, R., Aschmann, S. M., Fitz, D. R., Winer, A. M., and Pitts, J. N.: Rate constants for the gas-phase reactions of O3 with selected organics at 296 K, Int. J. Chem. Kinet., 14, 13-18, 1982.

Atkinson, R., Aschmann, S. M., and Carter, W. P.: Kinetics of the reactions of O3 and OH radicals with furan and thiophene at 298±2 K, Int. J. Chem. Kinet., 15, 51-61, 1983.

Atkinson, R., Baulch, D., Cox, R., Crowley, J., Hampson, R., Hynes, R., Jenkin, M., Rossi, M., Troe, J., and Subcommittee, I.: Evaluated kinetic and photochemical data for atmospheric chemistry: Volume II–gas phase reactions of organic species, Atmos. Chem. Phys., 6, 3625-4055, 2006.

Barker, G., Fowles, P., and Stringer, B.: Pulse radiolytic induced transient electrical conductance in liquid solutions. Part 2.—radiolysis of aqueous solutions of NO_3^-, NO_2^- and $Fe(CN)_6^{3-}$, J. Chem. Soc. Faraday Trans., 66, 1509-1519, 1970.

Berdnikov, V.: Catalytic activity of the hydrated copper ion in the decomposition of hydrogen peroxide, Russ. J. Phys. Chem., 47, 1060-1062, 1973.

Bertolotti, S. G., García, N. A., and Argüello, G. A.: Effect of the peptide bond on the singlet-molecular-oxygen-mediated sensitized photo-oxidation of tyrosine and tryptophan dipeptides. A kinetic study, Journal of Photochemistry and Photobiology B: Biology, 10, 57-70, 1991.

Bielski, B.: Evaluation of the reactivities of HO2/O2 with compounds of biological interest, Oxy Radicals and Their Scavenger Systems. G. Cohen and RA Greenwald (Editors), 1, 1-7, 1983.

Bielski, B. H. J., Cabelli, D. E., Arudi, R. L., and Ross, A. B.: Reactivity of HO_2/O_2^- radicals in aqueous solution, Journal of Physical and Chemical Reference Data, 14, 1041-1100, 1985.

Bilski, P., Holt, R. N., and Chignell, C. F.: Properties of singlet molecular oxygen O2 (1Δg) in binary solvent mixtures of different polarity and proticity, Journal of Photochemistry and Photobiology A: Chemistry, 109, 243-249, 1997.

Buxton, G. V., Greenstock, C. L., Helman, W. P., and Ross, A. B.: Critical review of rate constants for reactions of hydrated electrons, hydrogen atoms and hydroxyl radicals ($^{\cdot}$OH/$^{\cdot}$O^{-}) in aqueous solution, J. Phys. Chem. Ref. Data, 17, 513-886, 1988a.

Buxton, G. V., Wood, N. D., and Dyster, S.: Ionisation Constants of $^{\cdot}$OH And HO$^{\cdot}_{2}$ in Aqueous Solution up to 200°C. A Pulse Radiolysis Study, J. Chem. Soc., Faraday Trans., 84, 1113-1121, 1988b.

California Air Resources Board, iADAM database: Air Quality Data Statistics: https://www.arb.ca.gov/adam, access: June 6, 2018.

Canonica, S., Hellrung, B., and Wirz, J.: Oxidation of phenols by triplet aromatic ketones in aqueous solution, J. Phys. Chem. A, 104, 1226-1232, 2000.

Canonica, S., Kohn, T., Mac, M., Real, F. J., Wirz, J., and von Gunten, U.: Photosensitizer method to determine rate constants for the reaction of carbonate radical with organic compounds, Environmental science & technology, 39, 9182-9188, 2005.

Chen, S.-N., Hoffman, M. Z., and Parsons Jr, G. H.: Reactivity of the carbonate radical toward aromatic compounds in aqueous solution, J. Phys. Chem., 79, 1911-1912, 1975.

Chen, Z., Chu, L., Galbavy, E. S., Ram, K., and Anastasio, C.: Hydroxyl radical in/on illuminated polar snow: Formation rates, lifetimes, and steady-state concentrations, Atmos. Chem. Phys., 16, 9579-9590, 2016.

Deguillaume, L., Leriche, M., Monod, A., and Chaumerliac, N.: The role of transition metal ions on HO$_{x}$ radicals in clouds: a numerical evaluation of its impact on multiphase chemistry, Atmos Chem Phys, 4, 95-110, 2004.

Demerjian, K. L.: The mechanism of photochemical smog formation, Adv. Environ. Sci. Technol., 4, 1-262, 1974.

Hess, M., Koepke, P., and Schult, I.: Optical properties of aerosols and clouds: The software package OPAC, Bulletin of the American meteorological society, 79, 831-844, 1998.

Hoigné, J., and Bader, H.: Rate constants of reactions of ozone with organic and inorganic compounds in water—II: dissociating organic compounds, Water Res., 17, 185-194, 1983.

Huang, J., and Mabury, S. A.: Steady-state concentrations of carbonate radicals in field waters, Environmental Toxicology and Chemistry, 19, 2181-2188, 2000.

Hunter, T.: Radiationless transition T 1→ S 0 in aromatic ketones, Transactions of the Faraday Society, 66, 300-309, 1970.

Jen, C. N., Hatch, L. E., Selimovic, V., Yokelson, R. J., Weber, R., Fernandez, A. E., Kreisberg, N. M., Barsanti, K. C., and Goldstein, A. H.: Speciated and total emission factors of particulate organics from burning western US wildland fuels and their dependence on combustion efficiency, Atmos. Chem. Phys., 19, 1013-1026, 2019.

Kaur, R., and Anastasio, C.: Light absorption and the photoformation of hydroxyl radical and singlet oxygen in fog waters, Atmos. Environ., 164, 387-397, 2017.

Kaur, R., and Anastasio, C.: First measurements of organic triplet excited states in atmospheric waters, Environ. Sci. Technol., 52, 5218-5226, 2018.

Kozmér, Z., Arany, E., Alapi, T., Takács, E., Wojnárovits, L., and Dombi, A.: Determination of the rate constant of hydroperoxyl radical reaction with phenol, Radiat. Phys. Chem., 102, 135-138, 2014.

Lauraguais, A., Coeur-Tourneur, C., Cassez, A., and Seydi, A.: Rate constant and secondary organic aerosol yields for the gas-phase reaction of hydroxyl radicals with syringol (2, 6-dimethoxyphenol), Atmos. Environ., 55, 43-48, 2012.

Lilie, J.: Pulsradiolytische untersuchung der oxydativen ringöffnung von furan, thiophen und pyrrol/pulsradiolytic investigations of the oxydativ ring scission of furan, thiophen and pyrrol, Zeitschrift für Naturforschung B, 26, 197-202, 1971.

McGregor, K. G., and Anastasio, C.: Chemistry of fog waters in California's Central Valley: 2. Photochemical transformations of amino acids and alkyl amines, Atmos. Environ., 35, 1091-1104, 2001.

Meylan, W. M., and Howard, P. H.: Computer estimation of the atmospheric gas-phase reaction rate of organic compounds with hydroxyl radicals and ozone, Chemosphere, 26, 2293-2299, 1993.

Neta, P., and Schuler, R. H.: Rate constants for reaction of hydrogen atoms with aromatic and heterocyclic compounds. Electrophilic nature of hydrogen atoms, Journal of the American Chemical Society, 94, 1056-1059, 1972.

O'Neill, P., Steenken, S., and Schulte-Frohlinde, D.: Formation of radical cations of methoxylated benzenes by reaction with OH radicals, Ti 2+, Ag 2+, and SO 4.-in aqueous solution. An optical and conductometric pulse radiolysis and in situ radiolysis electron spin resonance study, Journal of Physical Chemistry, 79, 2773-2779, 1975.

O'Neill, P., and Steenken, S.: Pulse radiolysis and electron spin resonance studies on the formation of phenoxyl radicals by reaction of OH radicals with methoxylated phenols and hydroxybenzoic acids, Ber. Bunsenges. Phys. Chem., 81, 550-556, 1977.

Parworth, C. L., Young, D. E., Kim, H., Zhang, X., Cappa, C. D., Collier, S., and Zhang, Q.: Wintertime water-soluble aerosol composition and particle water content in Fresno, California, J. Geophys. Res. Atmos., 122, 3155-3170, 2017.

Piechowski, M. V., Nauser, T., Hoignè, J., and Bühler, R. E.: O− 2 decay catalyzed by Cu2+ and Cu+ ions in aqueous solutions: a pulse radiolysis study for atmospheric chemistry, Berichte der Bunsengesellschaft für physikalische Chemie, 97, 762-771, 1993.

Rehorek, D., and Seidel, A.: A. Leifer. The kinetics of environmental aquatic photochemistry. ACS professional and reference book. American Chemical Society, Washington 1988, 304 S., 41 Abb., 35 Tab., Kart, Preis: US & Canada $59.95, Export $71.95, ISBN 0-8412-1464-6, Cryst. Res. Technol., 24, 732-732, 1989.

Richards-Henderson, N. K., Hansel, A. K., Valsaraj, K. T., and Anastasio, C.: Aqueous oxidation of green leaf volatiles by hydroxyl radical as a source of SOA: Kinetics and SOA yields, Atmos. Environ., 95, 105-112, 2014a.

Richards-Henderson, N. K., Pham, A. T., Kirk, B. B., and Anastasio, C.: Secondary organic aerosol from aqueous reactions of green leaf volatiles with organic triplet excited states and singlet molecular oxygen, Environ. Sci. Technol., 49, 268-276, 2014b.

Rinke, M., and Zetzsch, C.: Rate Constants for the Reactions of OH Radicals with Aromatics: Benzene, Phenol, Aniline, and 1, 2, 4-Trichlorobenzene, Ber. Bunsenges. Phys. Chem., 88, 55-62, 1984.

Rosario-Ortiz, F. L., and Canonica, S.: Probe compounds to assess the photochemical activity of dissolved organic matter, Environ. Sci. Technol., 50, 12532-12547, 2016.

Seinfeld, J. H., and Pandis, S. N.: Atmospheric chemistry and physics: From air pollution to climate change, John Wiley & Sons, 2012.

Smith, J. D., Sio, V., Yu, L., Zhang, Q., and Anastasio, C.: Secondary organic aerosol production from aqueous reactions of atmospheric phenols with an organic triplet excited state, Environ. Sci. Technol., 48, 1049-1057, 2014.

Smith, J. D., Kinney, H., and Anastasio, C.: Aqueous benzene-diols react with an organic triplet excited state and hydroxyl radical to form secondary organic aerosol, Phys. Chem. Chem. Phys., 17, 10227-10237, 2015.

Solar, S., Solar, W., and Getoff, N.: Reactivity of hydroxyl with tyrosine in aqueous solution studied by pulse radiolysis, J. Phys. Chem., 88, 2091-2095, 1984.

Tetreau, C., Lavalette, D., Land, E., and Peradejordi, F.: Sensitized triplet-triplet absorption of biphenylene, Chem. Phys. Lett., 17, 245-247, 1972.

Tratnyek, P. G., and Hoigne, J.: Oxidation of substituted phenols in the environment: A QSAR analysis of rate constants for reaction with singlet oxygen, Environ. Sci. Technol., 25, 1596-1604, 1991a.

Tratnyek, P. G., and Hoigne, J.: Oxidation of substituted phenols in the environment: a QSAR analysis of rate constants for reaction with singlet oxygen, Environmental science & technology, 25, 1596-1604, 1991b.

USEPA: Estimation Programs Interface Suite™ for Microsoft® Windows, v 4.11, United States Environmental Protection Agency, Washington, DC, USA, 2012.

USGS: U.S. Geological Survey. Water Properties - Dissolved Oxygen. Available at https://water.usgs.gov/edu/dissolvedoxygen.html [last accessed: January 23, 2018], 2018.

Vempati, H. S.: Physico-chemical properties of green leaf volatiles, 2014.

Vione, D., Minella, M., Maurino, V., and Minero, C.: Indirect photochemistry in sunlit surface waters: photoinduced production of reactive transient species, Chemistry-A European Journal, 20, 10590-10606, 2014.

Wilkinson, F., Helman, W. P., and Ross, A. B.: Quantum yields for the photosensitized formation of the lowest electronically excited singlet state of molecular oxygen in solution, J. Phys. Chem. Ref. Data, 22, 113-262, 1993.

Wilkinson, F., Helman, W. P., and Ross, A. B.: Rate constants for the decay and reactions of the lowest electronically excited singlet state of molecular oxygen in solution. An expanded and revised compilation, J. Phys. Chem. Ref. Data, 24, 663-677, 1995.

Yasuhisa, T., Hideki, H., and Muneyoshi, Y.: Superoxide radical scavenging activity of phenolic compounds, International journal of biochemistry, 25, 491-494, 1993.

Young, D. E., Kim, H., Parworth, C., Zhou, S., Zhang, X., Cappa, C. D., Seco, R., Kim, S., and Zhang, Q.: Influences of emission sources and meteorology on aerosol chemistry in a polluted urban environment: results from DISCOVER-AQ California, Atmos. Chem. Phys., 16, 5427-5451, 2016.

Zein, A. E., Coeur, C. c., Obeid, E., Lauraguais, A. l., and Fagniez, T.: Reaction kinetics of catechol (1, 2-benzenediol) and guaiacol (2-methoxyphenol) with ozone, The Journal of Physical Chemistry A, 119, 6759-6765, 2015.

Zeng, T., and Arnold, W. A.: Pesticide photolysis in prairie potholes: probing photosensitized processes, Environmental science & technology, 47, 6735-6745, 2012.

Zepp, R. G., Braun, A. M., Hoigne, J., and Leenheer, J. A.: Photoproduction of hydrated electrons from natural organic solutes in aquatic environments, Environmental science & technology, 21, 485-490, 1987.

Zhou, X., and Mopper, K.: Determination of photochemically produced hydroxyl radicals in seawater and freshwater, Mar. Chem., 30, 71-88, 1990.